Ecolé Polytechnique Féderale de Lausanne - EPFL

Environmental Microbiology Laboratory- EML

HEXAVALENT URANIUM REDUCTION AND FRACTIONATION BY THE MODEL METAL-REDUCING BACTERIUM *SHEWANELLA ONEIDENSIS*

MSc Thesis

Environmental Sciences & Engineering

Camila Morales Undurraga

Supervisor:
Prof. Dr. Rizlan Bernier-Latmani
Dr. Ashley Brown

August 5, 2022

Acknowledgements

I would like to express my gratitude to my supervising professor, Prof. Dr. Rizlan Bernier-Latmani, for contributing to this study with her considerable expertise and giving me the opportunity to work in the Environmental Microbiology Laboratory at EPFL.

I would particularly like to thank my direct supervisor, Dr. Ashley Brown, for his constant supervision, motivation, and encouragement in carrying out this thesis. His guidance and specific knowledge helped me in all the time of lab work, research, and writing, giving me the confidence needed to work on such a challenging topic. With his professional and moral support, I could not have imagined a better advisor and mentor for this thesis.

I would like to extend my thanks to Dr. Karin Meibom, who helped us to generate the strains used in this project, to Dr.Yvonne Roebbert and Dr. Stefan Weyer that helped us with the isotope analysis. Without their support, this thesis would not have been possible.

I want to thank all the beautiful friends that I have made through this journey here in Switzerland, that made me feel this place like home.

I would like to recognize my siblings, who have given me moral support when being 12.000 km apart. I cannot fail to also mention my uncle, Hugo, without your support none of this would have been possible.

I owe my deepest gratitude to Gabriel, that has been here for me every single time that I needed support, care, and companionship. I could not have made it this far if it was not for you.

Finally, I would like to dedicate this achievement to my mom. Thank you for being my guiding light, for inspiring me, and for influencing my life for the better, you are the main reason why I am here today.

Lausanne, August 5, 2022

Camila Morales Undurraga

Abstract

Uranium is a widespread environmental contaminant [1] that in natural environments is predominantly found in the U(IV) and U(VI) forms. This radionuclide in its oxidized form U(VI) typically forms stable complexes, resulting in highly soluble and mobile species [2], whilst the reduction of U(VI) to U(IV) leads to the precipitation of uraninite (UO_2) and other non-crystalline species [3][4][5].

In this sense, bioremediation through the stimulation of certain bacteria, such as *Shewanella oneidensis* MR-1, is a promising and inexpensive solution to remediate radionuclide contamination. Its strategy is based on the use of *c*-type cytochromes, as electron transfer proteins, allowing it to couple the oxidation of organic matter to the extracellular reduction of several redox-active metals and radionuclides [6][7].

However, this solution needs a monitoring strategy in order to confirm that U(VI) has been successfully removed from groundwater, and remains stable through time. A straightforward approach would be to directly measure U(VI) concentration, but such data may be subject to artefacts arising from hydrochemical effects, such as dilution after a rainfall event or adsorption of U(VI) onto aquifer mineral phases. Based on this, $^{238}U/^{235}U$ isotope ratios offer an advanced monitoring tool, since it is well known that bacterial reduction of soluble U(VI) leads to preferential partitioning of the heavy isotope ^{238}U in the U(IV) solids [8][9].

Therefore, this study aims to determine the impact of U(VI)-edta reduction rates on isotopic fractionation of uranium. To this end, a set of key components of the electron transport network of *Shewanella oneidensis* MR-1, such as the global *c*-type cytochrome concentration and the expression level of CymA, Fdh and MtrCAB proteins were explored to determine their effects on U(VI)-edta reduction rate and ultimately, isotopic fractionation.

The results obtained in this study showed that there is a direct relationship between *c*-type cytochrome concentration and U(VI)-edta reaction rate, indicating that the anaerobic growth regime of *S.oneidensis* MR-1 can impact the reaction through varied expression levels of *c*-type cytochromes. Additionally, it was found that the expression level of the MtrCAB conductive complex is rate limiting during U(VI)-edta reduction, consistent with previous findings [10]. Finally, this study shows that isotopic fractionation of uranium is impacted by reaction rate with stronger fractionation observed for slower reactions. However, this explicit relationship appears to be governed by the relative availability of the U(VI) substrate with respect to MtrC levels rather than the absolute reaction rate itself.

Key words: U(VI) reduction, bioremediaton, *Shewanella oneidensis* MR-1, *c*-type cytochrome, uranium isotopic fractionation.

Résumé

L'Uranium est un contaminant environnemental répandu [1] qui, dans les environnements naturels, se trouve principalement sous les formes U(IV) et U(VI). Sous sa forme oxydée, ce radionucléide oxydée (U(VI) forme typiquement des complexes stables, résultant en des espèces hautement solubles et mobiles [2], tandis que la réduction de U(VI) en U(IV) conduit typiquement à la précipitation d'uraninite (UO2) et d'autres espèces non cristallines [3][4][5].

En ce sens, la bioremédiation par la stimulation de certaines bactéries, telles que *Shewanella oneidensis* MR-1, est une solution prometteuse et peu coûteuse pour remédier à la contamination par les radionucléides. Sa stratégie repose sur l'utilisation de cytochromes de type-*c*, comme protéines de transfert d'électrons, lui permettant de coupler l'oxydation de la matière organique à la réduction extracellulaire de plusieurs métaux et radionucléides redox-actifs [6][7].

Cependant, cette solution nécessite une stratégie de surveillance afin de confirmer que l'U(VI) a été éliminé avec succès des eaux souterraines et reste stable dans le temps. Une approche simple consisterait à mesurer directement la concentration en U(VI), mais ces données peuvent être sujettes à des artefacts résultant d'effets hydrochimiques, tels que la dilution après un événement pluvieux ou l'adsorption d'U(VI) sur les phases minérales de l'aquifère. Sur cette base, les rapports isotopiques $^{238}U/_{235}U$ offrent un outil de surveillance avancé, car il est bien connu que la réduction bactérienne de l'U(VI) soluble conduit à une répartition préférentielle de l'isotope lourd $_{238}U$ dans les solides U(IV) [8][9]

Ainsi, cette étude vise à déterminer l'impact des taux de réduction de l'U(VI)-edta sur le fractionnement isotopique de l'uranium. À cette fin, un ensemble de composants clés du réseau de transport d'électrons de *Shewanella oneidensis* MR-1, tels que la concentration globale de cytochrome de type- *c* et le niveau d'expression des protéines CymA, Fdh et MtrCAB, ont été explorés pour déterminer leurs effets sur le taux de réduction de l'U(VI)-edta et, finalement, le fractionnement isotopique.

Les résultats obtenus dans cette étude ont montré qu'il existe une relation directe entre la concentration de cytochrome de type-*c* et le taux de réaction U(VI)-edta, indiquant que le régime de croissance anaérobique de *S. oneidensis* MR-1 peut impacter la réaction à travers des niveaux d'expression variés des cytochromes. Par ailleurs, il a été constaté que les niveaux d'expression du complexe conducteur MtrCAB sont limitants lors de la réduction de l'U(VI)-edta, en cohérence avec une étude précédente [10]. Enfin, cette étude montre que le fractionnement isotopique de l'uranium est impacté par la vitesse de réaction, avec un fractionnement plus fort observé pour une réaction plus lente. Cependant, cette relation

explicite semble régie par la disponibilité relative du substrat U(VI) par rapport aux niveaux de MtrC plutôt que par la vitesse de réaction absolue elle-même.

Mots clés : réduction U(VI), biorestauration, *Shawenella oneidensis* MR-1, cytochrome de type-*c*, fractionnement isotopique de l'uranium.

Contents

List of Figures

List of Tables

Chapter 1

Introduction

Uranium (U) is a naturally occurring radioactive element, present in various physical and chemical forms in the Earth's crust [13]. Research into U biogeochemistry has received significant attention in the last decades due to anthropogenic activities such as nuclear research, fuel production, and weapons manufacturing, resulting in widespread environmental contamination of this radionuclide [1]. Unfortunately, this worldwide phenomena poses a significant problem due to the radiological and chemical toxicity of this element [13].

Oxidation states of uranium range from +3 to +6, however, in natural environments uranium is predominantly found in the U(IV) and U(VI) forms. Under the redox conditions found in nature, dissolved U(III) readily oxidizes to U(IV), whereas dissolved U(V) spontaneously disproportionates to U(IV) and U(VI) [14]. The environmental behavior of this radionuclide is driven by its redox chemistry, where in its oxidized form (U(VI)), UO_2^{2+} typically forms stable complexes, for example with carbonate, resulting in highly soluble and mobile species [2]. On the other hand, the reduction of U(VI) to U(IV) typically leads to the precipitation of uraninite (UO_2) and other non-crystalline species, complexed by carbonate, phosphate and humic substances, for example [3][4][5].

Due to the high solubility and mobility of U(VI), groundwater contamination is extensive worldwide and prohibitively expensive to remediate with traditional strategies [15]. However, bioremediation through the stimulation of the native/indigenous subsurface bacteria capable of the reductive precipitation of metals, is a promising and inexpensive solution to remediate radionuclide contamination [16]. Nonetheless, this strategy, as any other, needs monitoring to confirm that U(VI) has been successfully removed from groundwater, and remains stable through time. Typically, this involves the collection and measurement of aqueous U concentrations in several monitoring wells downstream from the site of remediation. Whilst this represents a straight-forward approach, such data may be subject to artefacts arising from

hydrochemical effects, such as dilution after a rainfall event or adsorption of U(VI) onto aquifer mineral phases, for example. Both these processes result in an apparent decrease in aqueous U concentrations, but not via the desired reductive precipitation of a stable immobile U(IV) species. Hence, in the case of adsorption, changes to groundwater chemistry may result in extensive re-mobilization of sorbed U(VI).

Based on the aforementioned, changes in $^{238}U/^{235}U$ isotope ratios, arising from isotope fractionation, offer an advanced monitoring tool. Here, fractionation refers to the relative partitioning of the heavier and lighter isotopes between two coexisting phases in a natural system [17] whose process, in the case of U, is strongly driven by redox transformations [18].

Uranium in nature is mainly present as the ^{238}U and ^{235}U isotopes , with natural abundances of (99.27%) and (0.72%), respectively [1]. When it comes to bioremediation of U(VI), it is well known that bacterial reduction of soluble U(VI) leads to preferential partitioning of the heavy isotope ^{238}U in the U(IV) solids [8][9].This phenomena, contrary to what is commonly observed for light elements, is caused by differences in nuclear sizes and shapes of isotopes, described in the literature as the nuclear field shift effect (NFSE) [19][20]. This results in the heavy isotope being more stable in the species with the lowest electron density at the nucleus, in the case of uranium, this is the reduced U(IV) oxidation state.

The isotopic fractionation between U(VI) and U(IV) is described by the fractionation factor (α) and isotopic ratios are reported in delta δ notation relative to a standard. Additionally, the magnitude of U isotope fractionation is generally expressed as the enrichment factor (ε) [8].

$$\alpha = \frac{R_{U(VI)}}{R_{U(IV)}} \tag{1.1}$$

$$R = \frac{^{238}U}{^{235}U} \tag{1.2}$$

$$\delta^{238}U(VI) = \frac{R_{U(VI)}^{238/235} - R_{STD}^{238/235}}{R_{STD}^{238/235}} \tag{1.3}$$

$$\varepsilon(‰) = 1000 * (\alpha - 1) \tag{1.4}$$

Uranium isotope fractionation occurs at the permil-level and isotope ratios have been widely applied as a redox proxy in studies of paleo-climate in ancient environments[21][22][23][24]. This has led U isotope fractionation to being considered as a monitoring tool for modern

contaminated land [18]. For example, a recent study at the Rifle Integrated Field Research Challenge Site in Rifle, Colorado measured U isotopic fractionation after a bioremediation experiment, showing a significant ∼1‰ decrease in $^{238}U/^{235}U$ as the U(VI) concentration decreased [25]. In this manner, as uranium reduction leads to the enrichment of heavy U isotopes in the U(IV) solid phase, then light U isotope signatures in the aqueous phase may indicate uranium reduction, consistent with that expected for biological reduction[18]. Furthermore, it is also well studied that $^{238}U/^{235}U$ in groundwater is not significantly impacted by bicarbonate-induced desorption of U(VI) from mineral surfaces or by the adsorption of U(VI) on those surfaces [26][5]. Given that U(VI) removal from water by natural and stimulated reductive pathways is the dominant source of U isotopic fractionation [26], these studies collectively suggest that U isotope signatures may present a reliable tool to complement U(VI) concentration measurements.

1.1 The metal-reducing bacterium *Shewanella oneidensis*

A wide range of microorganisms from contaminated sites that can immobilize uranium have been identified [13]. The microbial interaction with this radionuclide leads to the sequestration or complexation of uranium, resulting in a decrease of its aqueous concentration in the environment

Nowadays, *Shewanella oneidensis* MR-1, a dissimilatory metal-reducing bacteria (DMRB), is one of the best understood models to study extracellular electron transfer (EET) processes. Its strategy is based on the use of *c*-type cytochromes, as electron transfer proteins, allowing it to couple the oxidation of organic matter to the extracellular reduction of several redox active metals and radionuclides [6][7]. This makes them especially attractive for bioremediation proposes.

This organism, under anaerobic conditions, has the capacity to reduce a wide range of organic and inorganic substrates, such as fumarate, nitrate, thiosulfate, as well as soluble metal complexes or metals associated with solid phase minerals, such as uranium, cobalt, vanadium, among others [27]. This interesting ability to reduce a variety of electron acceptors is associated with the diverse respiratory network of *S. oneidensis*, where *c*-type cytochromes play an essential role.

Several studies have shown that *S. oneidensis* contains 42 putative *c*-type cytochromes [28][29]. However, only a few of them are identified as a key components during metal re-

duction, which has been shown to occur via the Mtr pathway, whose five primary protein components have been identified: OmcA, MtrC, MtrA, MtrB, and CymA [30]. Figure 1.1 illustrates a modified respiratory pathway model previously suggested by other authors [10][11]. In this figure, lactate represents both the carbon source, and electron donor for respiration by *S. oneidensis*. When electrons are generated during the metabolism of lactate, they are stored in the form of NADH, which is the intracellular electron carrier. Subsequently, these electrons are transferred from NADH to the outer membrane (OM) through the menaquinol pool and the already mentioned *c*-type cytochromes, including OmcA-MtrCAB and CymA. Finally electrons are released to the extracellular electron acceptor, in this case U(VI) [10][31].

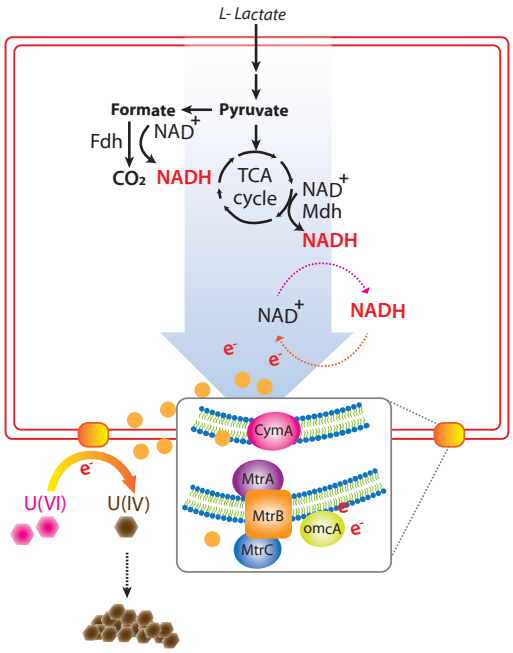

Figure 1.1: Model for possible electron transport pathways of *S. oneidensis*, from electron carbon source to electron release for U(VI) reduction. Membranes representation emphasizes CymA in the inner membrane and MtrA exposed to the periplasm, MtrB, MtrC and OmcA located in the outer membrane. This model corresponds to a modification of the one proposed by Fan et al., (2021) [10] including a new arrangement of the MtrCAB complex as proposed by Edwards et al.,(2020) [11].

There are several proposed mechanisms for U(VI) reduction, which vary greatly among microorganisms, suggesting that there are no unique proteins specifically for uranium reduction [32] . Nevertheless, it is well established that U(VI) reduction occurs via 2 electrons released by the microorganism or via one electron, forming U(V) which ultimately could be reduced to U(IV) via a second successive electron transfer or via disproportionation of U(V) to U(VI) and U(IV) [2] [33]. Regarding the stability of U(IV) products, the formation of

uraninite or noncrystalline U(IV) seems to be correlated to the chemical speciation of the medium where reaction occurs [4][18]. It is suggested that non-crystalline forms of U(IV) may be more labile than uraninite [34] and, therefore more likely to be re-oxidized. Consequently, U(IV) can be remobilized by the presence of certain oxidants or complexation with organic ligands, such as citrate and Ethylenediaminetetraacetic acid (edta), which are present in the environment either naturally or due to its use in processing of radioactive waste, respectively; both being capable of forming stable and strong complexes [18].

The U(VI) reduction capacity of *S. oneidensis*, represented by the reaction rate (k), is governed by several factors. In this line, the importance of *c*-type cytochromes on reduction rate has been highlighted by studies of azo dye reduction by this bacteria [35]. However, the impact of uranium on reaction rate remains uninvestigated.

Additionally, it has been shown that components, other than *c*-type cytochromes, govern the reduction rate of *S. oneidensis*. In this sense, studies have shown that proteins, such as Mdh and Fdh, the latter being responsible of formate oxidation in the repiratory cycle of *S. oneidensis* [36], may also be rate limiting during U(VI) reduction [10]. Similar findings have been reported for key *c*-type cytochromes, such as cymA and the MtrCAB complex, showing significant differences in reaction rate when these proteins are overexpressed [10].

There is a clear requirement to understand the role that key proteins have in controlling U(VI) reduction rate, and subsequently the control that this exerts over fractionation magnitude. A systematic understanding of these process would provide the mechanistic basis for interpreting isotopic signatures measured during bioremediation, and may ultimately lead to the deployment of isotopic signatures as a quantitative tool.

1.2 Aims & Objectives

Aim

The main aim of this work was to determine the impact of reduction rate on isotopic fractionation of uranium. To this end, the effect of variable expression of key components of the electron transport network of *Shewanella oneidensis* MR-1 on U(VI)-edta reduction rate was explored.

Objectives

In order to address the aforementioned aim, this work focused on four specific objectives

1. Determine the impact of varying electron donor–acceptor ratios during growth on *c*-type cytochrome expression, and subsequently on U(VI) reduction rates, as it has been previously done for azo dye reduction [35].

2. Elucidate whether CymA and Fdh proteins represent rate-limiting steps in the U(VI) reduction, via their overexpression.

3. Control the expression of the mtrCAB complex, via the introduction of the araC-p_{BAD} promoter system, to systematically vary extracellular electron flux.

4. Finally, by selection of systems displaying varied electron transfer rates, attempt to mechanistically relate U(VI) reduction rates to observed isotope fractionation factors.

Chapter 2

Materials and Methods

2.1 Varying *c*-type cytochrome concentration via different electron donor-acceptor ratios

In this section, the impact of changing electron donor–acceptor ratios on *c*-type cytochromes in the bacterium *Shewanella oneidensis*, using batch cultures was investigated.

Anaerobic minimal medium preparation:

An anaerobic minimal medium including an amino acid solution (20 mg/L L-arginine hydrochloride, 20 mg/L L-glutamate and 20 mg/L L-serine) was prepared as previously described [35]. Five media with different electron donor-acceptor ratios were prepared in total (Table 2.1). The electron donor corresponded to Sodium DL-lactate while fumarate was used as the electron acceptor. The pH was adjusted to 7.8 and the medium was then transferred into 80 mL serum bottles, capped with a butyl stopper and aluminium crimp and then autoclaved. Finally all bottles were sparged with N_2 for 30 minutes.

Table 2.1: Sodium DL-lactate and fumarate concentrations used for each medium with different ratios of electron donor-acceptor. The numbers in the notation of each ratio correspond to mM of lactate and fumarate, respectively. For example L100F20 refers to a medium with 100 mM of lactate and 20 mM of fumarate.

Ratio	**DL-lactate [mM]**	**fumarate [mM]**
L100F20	100	20
L70F50	70	50
L50F50	50	50
L50F70	50	70
L20F100	20	100

Inoculation procedure:
S. oneidensis MR-1 strain was obtained from the EPFL-Environmental Microbiology group culture collection stored at -80 °C. The cultures used were grown in the fully defined minimal medium previously described. The inoculation procedure consisted of the following three steps:

1. Inoculation into starting oxic media: An Erlenmeyer flask cointaning 50 mL L100F20 medium was unoculated with *S. oneidensis* MR-1 from LB agar using a sterile loop and placed in a shaking incubator (30°C and 140 rpm) for 1-2 days until the optical density at 600 nm (OD600) reached >1.

2. Inoculation into starting anaerobic bottle: An 80 mL anoxic serum bottle containing the defined medium for each lactate:fumarate ratio was inoculated from the oxic culture to obtain an initial OD600 of 0.02. The bottles were left to grow in the dark in a 30°C incubator for 2 days, without shaking.

3. Inoculation into main anaerobic growth medium: Three biological replicate bottles of 80 mL were inoculated from the starting anaerobic culture to obtain an initial OD600 of 0.02. This was done for each lactate:fumarate ratio. Again, the bottles were incubated at 30°C.

Biomass quantification:
The optical density at 600 nm (OD600) was measured approximately every four hours, using a Shimadzu spectrophotometer (Shimadzu UV-2501PC, Suzhou Instruments Manufacturing Co. Ltd., Suzhou, China). Three technical replicate measurements from each biological replicate were taken throughout the first 58 hours of incubation.

***c*-type cytochrome quantification:**
The *c*-type cyctochrome concentration for five different lactate:fumarate ratios was determined after 24 hours (when cultures had reached the maxium yield) by means of pyridine hemochrome analysis [37]. A stock solution containing 200 mM NaOH and 40% of pyridine was prepared. Then 0.5 mL of the stock solution was placed in a 1mL-cuvette along with 3µL of 0.1M Potassium ferricyanide ($K_3Fe[CN]_6$) solution. Subsequently, 0.5 mL aliquot of the sample (previously concentrated and lysed) was added to the cuvette and the oxidized spectrum from 520 to 620 nm was recorded using a Shimadzu spectrophotometer. Then, the reduced spectra (using same wavelength range) were recorded after adding 2-5 mg of sodium dithionite. The spectra were measured several times until no significant differences were observed. The first spectrum that did not show further changes with respect to the previously recorded spectrum was used for calculations.

The samples used for this method were harvested after 24 hours and they were concentrated to OD600 equal to 1 trough centrifugation followed by lysis of 1 mL aliquot using silica bead-beating homogenizer for 3 cycles of 1 minute.

Finally, for the calculation of *c*-type cytochrome concentration, the Beer-Lambert law was used. The difference between the absorption in the reduced (550 nm) and oxidized state (534 nm) was calculated by subtraction and a molar extinction coefficient of 23.97 $mM^{-1}cm^{-1}$ was used [37]. All determined values were normalized by total protein content, obtained via the BCA protein assay [38].

2.1.1 Impact of *c*-type cytochrome concentration on U(VI) reduction rate

The effect of *c*-type cytochrome concentrations on U(VI) reduction rate was studied after the anaerobic growth of the bacteria using three different lactate:fumarate ratios: 100 mM lactate and 20 mM fumarate (L100F20); 50 mM lactate and 50 mM fumarate (L50F50); 20 mM lactate and 100 mM fumarate (L20F100).

Samples preparation and cell harvesting

Anoxic minimal media for each lactate:fumarate ratio was prepared according to the method described in Section 2.1, albeit at a volume of 350 mL to provide enough biomass for U(VI)-reduction experiments. As before, cultures were pre-grown in oxic minimal medium, followed by subculturing into anoxic minimal media. After approximately two days, 500 mL bottles containing 350 mL of anoxic medium, were inoculated from the anoxic starter culture to give an initial OD600 of 0.02. The cultures were then incubated at 30°C for 24 hours.

Cells were harvested after 24h, when previous growth experiments indicated all cultures had reached late log-early stationary phase. All cultures were transferred to an anoxic chamber and decanted into 500 mL anoxic centrifuge bottle. The bottles were centrifuged at 8000g for 15 minutes and moved back to the anoxic chamber, where the supernatant was discarded. The pellets were re-suspended in 200 mL PIPES-bicarbonate washing medium (Appendix A) and centrifuged again. Finally, after forming a pellet, this was re-suspended in PIPES-edta medium (Appendix A) to reach a final OD600 of 2.

U(VI) reduction

Three 1 mL reactors were prepared in total, one for each culture grown under each lactate-fumarate ratio. Every reactor contained 20 mM PIPES, 5 mM edta, 20 mM lactate and 200 µM U, added from a 0.1 N HCl stock. Before starting the reaction by adding cells, 50 µL of each reactor were sampled, corresponding to t_o in our analysis. Then, 50 µL of each culture was added into their respective reactors, giving a final OD600 of 0.1. Once the reaction initiated, the reactors were stored in darkness between each sampling point. This experiment was performed for two replicate, from cell grown in different batches.

Uranium oxidation state separation and analysis of U concentrations via ICP-MS

In order to measure U(VI) and U(IV) during the reaction, ion exchange chromatography was used to separate uranium oxidation states. The separation was performed under anaerobic conditions in an anoxic chamber, using polypolylene chromatography columns, which contained approximately 3 mL of an acidified suspension of Dowex 1x8 ion exchange resin. The Dowex 1x8 resin is a strongly basic cationic resin that allows anion separation in an HCl-acidified sample [2]. In this manner, in hydrochloric acid solutions of concentrations greater than 3.5 M, U(VI) forms anionic chloro-complexes, which are strongly adsorbed to the resin. On the other hand, U(IV) remains as a cation and is not adsorbed in concentration of HCl lower than 5.5 M [39].

Briefly, at appropriate time intervals, 50 µL of sample from each reactor was added into the column that was previously conditioned with 4.5 N HCl. The columns were then flushed with 10 bed volumes (30 mL in total) of 4.5 N HCl to elute the U(IV)-containing fraction. Subsequently, the U(VI)-containing fraction was eluted using 10 bed volumes of 0.1 N HCl.

Finally, U(VI) and U(IV) concentrations were measured using Inductively Coupled Plasma Mass Spectrometry (ICP-MS, Perkin-Elmer ELAN DRC 2).

2.2 Effect of targeted proteins expressions on U(VI) reduction rate

The effect of CymA and Fdh, as well as MtrCAB expressions on U(VI) reduction rates were studied by following the U(VI)-edta reduction by genetically engineered *S. oneidensis* MR-1 strains. A first experiment consisted of comparing the reduction rates of wild-type alone or with an extra copy of both, the *cymA* and *cymA+fdh* genes. A second experiment comprised a comparison of four different MtrCAB expression levels in *S. oneidensis* MR-1 by adding

the L-arabinose concentration dependent araC-P_{BAD} promoter system in front of the mtr operon.

2.2.1 Genetically engineered *S. oneidensis* MR-1 strains

Generation of CymA and CymAFdh MR-1 recombinant:

An extra copy of the *cymA* or *cymA* + *fdh* genes were given to *S. oneidensis* MR-1 through the insertion of a plasmid incorporating the Kanamycin resistance gene and the Tac-promoter for RNA replication. The introduction of the plasmid in the bacteria was aided via electroporation, in which a brief high voltage is discharged to make the membranes of the cell permeable. Once the plasmid was inserted, the strains were grown in the presence of Kanamycin, allowing only the growth of those cells harboring the plasmid, and IPTG that is responsible for triggering RNA replication via the Tac promoter system. The same procedure was followed for wild-type containing an empty plasmid, used as a control sample.

The wild-type, CymA and CymA+Fdh MR-1 recombinant strains were plated onto LB agar in the presence of Kanamycin. The plates were stored at 30°C for 1.5 days. Subsequently, the strains were inoculated into 10 mL LB containing Kanamycin and were left for approximately 15 hours in an incubator at 30°C and 140 rpm. Finally, the OD600 of this starter culture was measured and 0.5 mL was inoculated into 50 mL LB in the presence of Kanamycin and IPTG. These cultures were then incubated for approximately 5 hours at 30° and 140 rpm, before being harvested and washed for inoculation of U(VI)-edta containing reactors

Generation of the araC-P_{BAD}-mtr MR-1 strain

In order to systematically control MtrCAB complex expression levels, the P_{BAD} promoter system was used. This promoter is controlled by the AraC dimer protein and can initiate gene expressions in presence of L-arabinose.

The mechanism used by the P_{BAD} promoter is controlled by the AraC protein as Figure 2.1 illustrates. In absence of L-arabinose, AraC binds to the O_2 and I_1 half sites of the araBAD operon, forming a DNA loop that blocks transcription. Conversely, when L-arabinose is present, it binds to AraC, which releases from the O_2 site and binds to I_2 (adjacent to I_1). This process allows the DNA loop to be opened and transcription starts. In this manner, expression levels can be controlled by varying L-arabinose concentrations.

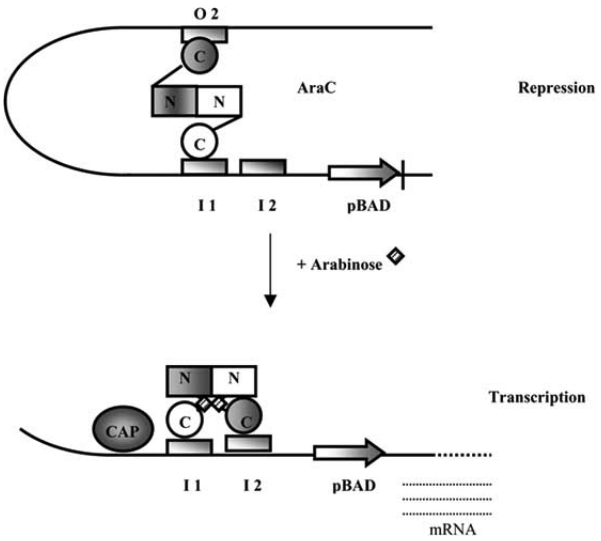

Figure 2.1: Schematic representation of the AraC-P_{BAD} promoter system controlled by the presence of L-arabinose [12].

Therefore, the AraC-P_{BAD} promoter system was integrated into the genome of *S. oneidensis* MR-1, replacing the natural promoter of MtrCAB complex. In order to place this system into the genome, a "suicide" plasmid containing AraC and the P_{BAD} promoter was inserted to the cell during growth in LB in presence of Kanamycin. The desired promoter was then incorporated into the genome by homologous recombination. Subsequently, sucrose was added to the medium to select only the strains with the P_{BAD} promoter system fully incorporated into the genome and without the residual redundant plasmid.

As for the cymA and CymA+Fdh strain, the P_{BAD} encoding MR-1 strain was plated onto LB agar at 30°C for 1.5 days. Then, one streak was transferred into an Erlenmeyer flask with 10 mL of LB and was incubated at 30°C and 140 rpm. After 15 hours, the OD600 was measured, and then four Erlenmeyer flasks containing 50 mL LB and different L-arabinose concentrations (0.1; 0.2; 0.4 and 1 mM), were inoculated to give an initial OD600 of 0.1. The flasks were then incubated for 5 hours at 30°C and 140 rpm.

The expression levels of the fours L-arabinose concentration systems were obtained by RT-qPCR, which allowed to obtain RNA concentrations for each system. The result are reported as expression ratio, using 0.1 mM L-arabinose system as the reference (i.e. for 0.1 mM expression ratio = 1).

2.2.2 Harvesting of cells and inoculation of U(VI)-edta containing reactors

After 5 hours of incubation, the OD600 was measured to confirm that growth was approximately 2.5. The cultures were shaken and transferred into 50 mL anoxic centrifuge tubes. Samples were centrifuged for 10 minutes at 500g and 16°C and supernatant was discarded.

The pellets and tubes were purged with N_2 before moving to the anoxic chamber. Once samples were in anoxic conditions, each pellet was re-suspended with 50 mL of PIPES-bicarbonate washing medium (Appendix A). The re-suspended pellets were centrifuged again under same conditions and were moved back to the anoxic chamber. The supernatant was discarded and pellets were re-suspended in appropriate volume of PIPES-edta medium (Appendix A) to reach a final OD600 of 20.

A 1 mL reactor for each strain was prepared, containing 20 mM PIPES, 5 mM edta, 20 mM lactate and 200 µM U, added from a 0.1 N HCl stock. Subsequently, 50 µL of each reactor were sampled, corresponding to t_o. The reaction was started by adding 50 µL of each re-suspended pellet of OD20 into their respective reactors. Samples were stored in darkness between each sampling point.

For cymA and CymA+Fdh experiment, the wild-type with an empty plasmid was used as a control. In the case of the MtrCAB strains, only the four L-arabinose concentration systems were considered. Each experiment was performed in two replicate from cells grown in separate batches.

Finally, once the reaction was initiated, different sampling time-points were considered for each experiment. The U(IV) and U(VI) separation was carried out using anion exchange resins as described previously.

2.2.3 Testing solubility of U-edta complex

In order to confirm the U-edta speciation and demonstrate that both U(VI) and U(IV) complexes are soluble, the following experiment was performed. An abiotic control sample containing U(VI) in 5 mM edta and a fully reduced sample from the MtrCAB experiment (containing 1 mM L-arabinose grown cells after at least 2 days) were used to test solubility of both uranium species. Both samples were filtered through 0.2 µm filter inside of the anoxic chamber. The uranium concentration of the filtered and non filtered sample (parent sample) was measured, corresponding to total U values. Subsequently, 50 µL of filtered samples were added to anion exchange resins columns to separate U(VI) and U(IV) and the concentration

of these species were measured for both the abiotic control and biotic sample (from MtrCAB experiment). Finally, with this experiment, we seek to demonstrate that there is not uranium losses due to precipitation and also that no reduction occurs in the control sample.

2.3 Isotope analysis

The isotopic $^{238}U/^{235}U$ composition of the remaining U(VI) at each time point of the 0.1 mM and 1.0 mM L-arabinose systems were analyzed. The analysis was performed at the Institute for Mineralogy at Leibniz Universität Hannover (Germany) using a Thermo-Finnigan Neptune multicollector ICP-MS (MC-ICP-MS). The results obtained from this analysis, corresponded to isotopic signature values ($\delta^{238}U(VI)$), which represent the relative difference of isotope ratios between a sample and the standard. (Chapter 1, Eq 1.3).

Then, to further characterize the uranium isotope fractionation, the isotopic signatures of the U(VI) fraction were used to fit the Rayleigh distillation model [18]:

$$\delta^{238}U(VI) = (\delta^{238}U(VI)_{to} + 1000)\frac{C}{C_0}^{(\alpha-1)} - 1000 \tag{2.1}$$

$$ln\left(\delta^{238}U(VI) + 1000\right) = (\alpha - 1) * ln\left(\frac{C}{C_0}\right) + ln\left(\delta^{238}U(VI)_{to} + 1000\right) \tag{2.2}$$

$$\varepsilon(‰) = 1000 * (\alpha - 1) \tag{2.3}$$

Here, $\delta^{238}U(VI)_{to}$ represents the initial U isotope composition of U(VI) and C/C_0 corresponds to the fraction of unreacted U(VI) respect to its initial concentration at t_0. In this manner, a Rayleigh behavior during U(VI) reduction is indicated by a straight line in a plot of $ln(C/C_0)$ vs $ln(\delta^{238}U + 1000)$, where the slope corresponds to (α - 1), which subsequently, allows the calculation of an isotope enrichment factor (ε)[18]. Finally, having $\delta^{238}U$ values from certain C/C_0 and knowing the reference value $\delta^{238}U_{to}$, the variables of this linear equation can be obtained and used to predict all $\delta^{238}U$ values from C/C_0 ranging from 0 to 1.

Chapter 3

Results and Discussions

In this section, the showed results correspond to the U(VI) reduction rates studied under different conditions. For all experiments presented in this report, uranium reduction was carried out using Ethylenediaminetetraacetic acid (edta) as an organic ligand. This compound has been widely used as a decontamination agent in nuclear facilities and therefore is found at relatively increased levels in radioactive wastes [40]. As edta is also able to form soluble, stable complexes with U(IV) [41], this compound represents a particular challenge for the remediation of contaminated land.

To determine uranium speciation in the experimental conditions implemented in this study, U(VI) speciation was modeled in form of Uranyl (UO_2^{2+}) in the presence of edta using MINEQL+ software.

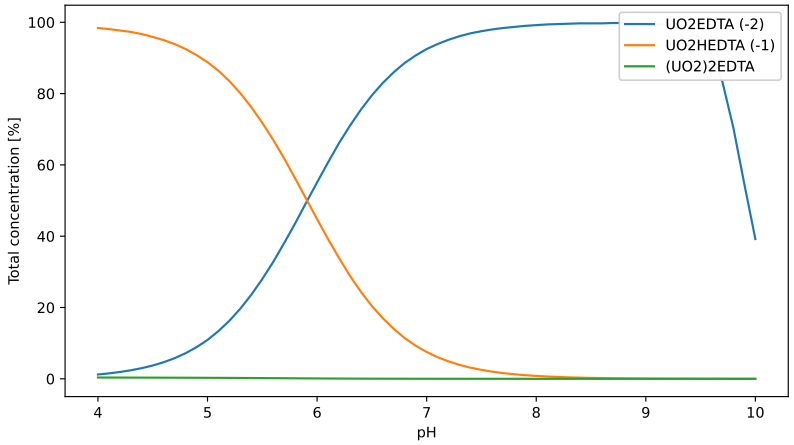

Figure 3.1: MINEQL+ model of U(VI)-edta speciation at different pH values under the following conditions: 200µM U(VI) and 5 mM edta.

Figure 3.1 shows UO_2^{2+} speciation in the presence of edta, indicating that at pH above 7, over 90% of the U(VI) is present in the form of UO_2-$EDTA^{2-}$ and the remaining 10% as UO_2H-$EDTA^{1-}$. This species distribution for uranyl(VI), is also found for edta concentrations as low as 0.2 mM and uranyl concentrations up to 0.5 mM (Appendix C.1; Figure C.1 and C.2). Hence, 200 µM of U and 5 mM of edta were the selected conditions for incubation with bacteria in the experiments shown in this study.

Similar results have been previously reported by other authors working with edta, where UO_2-$EDTA^{2-}$ corresponds to the predominant form of uranyl over pH 6 for an UO_2^{2+} concentration of 0.5 mM and edta of 2 mM [41]. This chemical speciation allows U(VI) in solution to be reduced to U(IV) in the aqueous form of U^{4+}–EDTA complex, preventing $U(IV)O_2$ precipitation during the reaction and maintaining all uranium in solution [42].

In order to demonstrate the aforementioned, a control sample containing U(VI)-edta was filtrated using a 0.2 µm filter and uranium concentration was measured, showing that the U concentration of the filtered sample was the same as non-filtered sample, confirming that U(VI)-edta remains soluble (Figure 3.2, left panel). Secondly, in order to confirm that the oxidation state corresponds to U(VI), ion exchange resin separation was used, showing that all uranium present in the filtered sample was indeed present as U(VI).

The same procedure was repeated using a U(IV) containing solution with 5 mM of edta. The sample was generated by biological reduction using *S. oneidensis* MR-1 and was left in the dark for one week. The parent sample was filtered and the uranium concentration was measured for both samples. The results shown in Figure 3.2, right panel, demonstrate that all U remained soluble and, ion exchange resin separation results showed that all uranium was present as U(IV) with negligible amounts of U(VI) detected.

Collectively, these data indicate that in the presence of 5 mM edta, incubation with bacteria results in the reduction of a soluble U(VI)-edta complex to a stable soluble U(IV)-edta complex, although the exact U(IV) speciation cannot be determined.

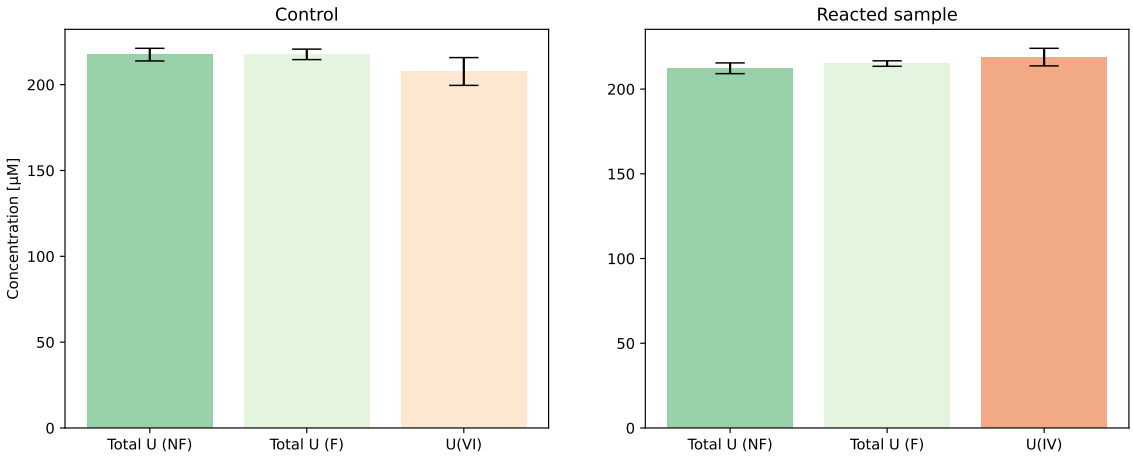

Figure 3.2: Uranium concentration obtained for a control (left panel) and and a reacted sample (right panel) in three different conditions: non filtrated (NF), filtrated (F), after resin separation (obtaining U(IV) and U(VI) separately). The error bars correspond to 2σ obtained from 4 different replicates for each sample.

3.1 Variable *c*-type cytochrome concentration

3.1.1 Varying *c*-type cytochrome concentration via different electron donor-acceptor ratios

The growth of *S. oneidensis* MR-1 using minimal medium containing different ratios of lactate (electron donor) and fumarate (electon acceptor) was followed during 58 hours and it is illustrated in Figure 3.3.

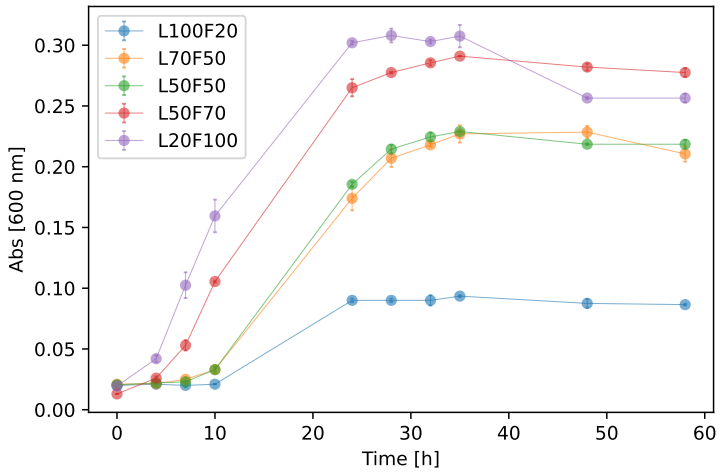

Figure 3.3: Anaerobic growth (OD600) of *S. oneidensis* MR-1 wild-type at different lactate(mM):fumarate(mM) ratios. The numbers in the notation correspond to mM of lactate:fumarate respectively. For instance, L100F20 refers to the medium containing 100 mM of lactate and 20 mM of fumarate. OD600 values correspond to the mean from 3 replicate and error bars to 2σ.

As it is possible to observe, the maximum yield was obtained for the system that was lactate limited (L20F100), reaching a maximum OD600 of 0.3. Moreover, the biomass yield is correlated with fumarate concentrations. This is exemplified by systems containing different lactate but the same fumarate concentrations (i.e. L70F50 and L50F50), showing same growth trend and yield despite differences in electron donor concentrations. For the fumarate limited system (L100F20), biomass yield was the lowest and only reached 30% of the maximum value obtained for L20F100.

Interestingly, biomass growth seems to be limited by fumarate concentration, in agreement with what is reported in literature regarding anaerobic growth of *S. oneidensis* [36]. According to authors, during this process each mole of lactate reduces two moles of fumarate, meaning that higher biomass is achieved when fumarate is present in sufficient concentrations, as was shown in these results.

Regarding their growth over time, all samples reached the stationary phase between 24-28 hours. Also, after 24 hours samples had different colors among them and the ones with lower biomass production had a pink color whereas the samples with the highest biomass showed a creamy color (Appendix D.1). According to a previous study, the pink color observed may be related to higher *c*-type cytochrome concentration when samples are grown under electron-acceptor limited conditions [35].

In order to quantify this, *c*-type cytochrome concentrations were determined via pyridine

hemochrome analysis [37], the obtained spectra for each system are shown in Appendix D.2. The *c*-type cytochrome concentrations normalized by total protein content are reported in Figure 3.4 and it shows that when *c*-type cytochrome concentrations are normalized there is a clear trend, where electron-acceptor limited samples present the greatest concentrations. This result is consistent with the previous observation, where samples with low fumarate concentration became pink, indicating higher *c*-type cytochrome concentrations for electron acceptor limited samples. These results are also consistent with those reported in the literature [35], where cellular *c*-type cytochrome concentrations showed a significant increase when lactate:fumarate ratios increased above 60 mM lactate: 60 mM fumarate.

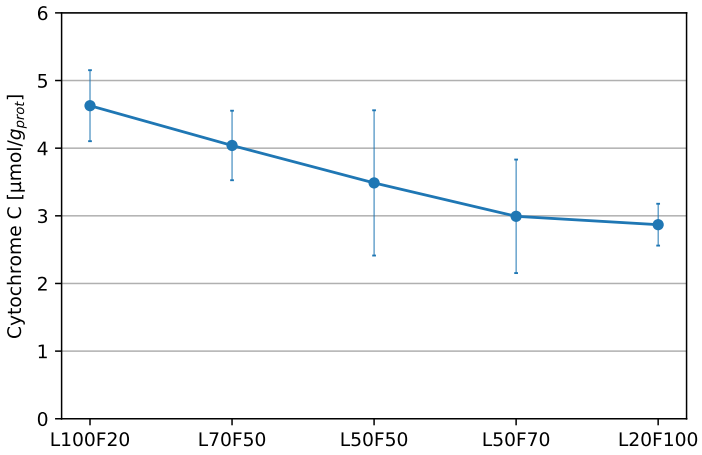

Figure 3.4: *c*-type cytochrome concentrations normalized to total protein content, for different lactate:fumarate ratios. Values correspond to the mean from three replicate and error bars to 2σ. The numbers in the notation correspond to mM of lactate:fumarate respectively. For instance, L100F20 refers to the medium containing 100 mM of lactate and 20 mM of fumarate.

The previous result of normalized *c*-type cytochrome concentrations supports the findings by Wang and et al. (2013) [35], where changes in electron donor-acceptor ratios impacted *c*-type cytochrome concentrations. Moreover, these authors showed that increasing *c*-type cytochrome concentrations enhanced azo dye reduction rates. Therefore, as *c*-type cytochromes have been implicated in the reduction of U(VI), we hypothesized that U(VI) reduction rates may also be impacted in a similar manner.

3.1.2 Impact of *c*-type cytochrome concentration on U(VI) reduction rate

To explore the effect of *c*-type cytochrome concentrations on reduction rates, three different ratios of lactate:fumarate were selected, the two end members: L100F20, L20F100; and the intermediate system: L50F50. Figure 3.5 and 3.6 show U(VI) reduction as a function of time and the first order reaction rates models, respectively, obtained for these three systems.

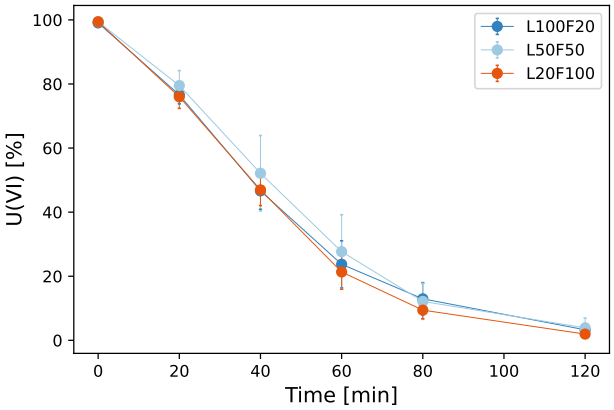

Figure 3.5: U(VI) reduction over time for *S. oneidensis* MR-1 wild-type grown in L100F20; L50F50 and L20F100 medium (numbers correspond to mM of lactate:fumarate respectively). Results correspond to the mean of replicate A and B, where error bars represent 2σ.

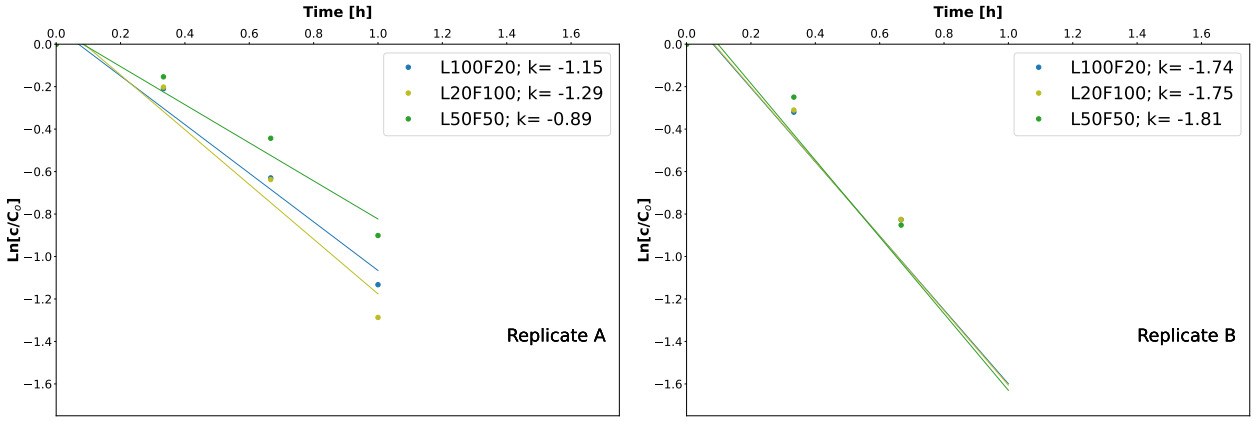

Figure 3.6: First order reaction rates of L100F20; L50F50; L20F100 (numbers correspond to mM of lactate:fumarate respectively) for replicate A (left) and B (right). Linear fitting was made using the first four time-points corresponding to 70% and 85% reduction for replicate A and B, respectively.

As it is possible to observe in Figure 3.5, U(VI) reduction reaction reached completion after two hours for the three systems used in this experiment and only minor differences can

be observed between them. Given that such systems resulted in significant differences in the reduction rate of azo dyes, it was expected to observe a similar effect here for U(VI).

It is well known that *c*-type cytochromes are the major component of the electron transport network of *S. oneidensis* MR-1, whose genome encodes up to 42 *c*-type cytochromes and among them, 15 correspond to membrane-bound *c*-type cytochromes [43]. Moreover, it is believed that *c*-type cytochromes located at the outer membrane (OM) are directly involved in the reduction of metals and radionuclides, such as U(VI) [27].

The results obtained in this experiment suggest that enhancing global concentrations of *c*-type cytochromes via different lactate:fumarate ratios does not lead to the increased expression of the rate-limiting cytochromes for U(VI) reduction. Thus, this method may be considered as a non-targeted approach for increasing *c*-type cytochrome concentrations and subsequent U(VI) reduction rates and it might be the reason of no significant differences in reaction rates for the three systems.

It is important to note that this experiment showed significant standard deviation (σ), especially for the first time-points, which might be the result of different *c*-type cytochrome expression levels obtained between replicate. For this reason, reaction rate results obtained for the three systems were normalized to protein content and are shown in Table 3.1.

Table 3.1: Normalized first order reaction rates (k) by total protein content for three systems with different lactate:fumarate ratios. In the notation, numbers correspond to mM of lactate:fumarate respectively. A and B correspond to the replicate.

	k [h^{-1}mg protein^{-1}]			
Sample	**A**	**B**	**mean**	**SD (σ)**
L100F20	-155.8	-168.3	-162.1	8.8
L50F50	-160.3	-108.8	-134.6	36.4
L20F100	-108.8	-102.6	-105.7	4.3

Table 3.1 shows that, despite the large standard deviation, especially for L50F50, significant differences in reaction rate were obtained for the two extreme cases L100F20 and L20F100, which is consistent with the trend in *c*-type cytochrome concentrations obtained in this experiment (Figure 3.4). Moreover, these results suggest that increasing *c*-type cytochrome concentration can enhance the ability of *S. oneidensis* to reduce U(VI) after growth under conditions of electron acceptor (fumarate) limitation, showing that the previous findings for azo dye reduction [35] are consistent with those for U(VI) reduction.

However, it is important to highlight that azo dye reduction rate was 10-fold higher for L100F20 compared to L20F100 [35], whereas U(VI) reduction in this experiment was only 1.5-fold higher for the same systems. The differences observed might be attributed to the reaction mechanism involved in azo dye and U(VI) reduction, which has been shown to be extracellular in both cases [27][44]. Nevertheless, we can not rule out the possibility that *c*-type cytochromes involved in azo dye reduction are not the same as for U(VI) reduction. In the same line, it is also possible that *c*-type cytochromes that are rate limiting for U(VI) reduction did not show increased expression. Additionally, these results may also be explained by the differences of *c*-type cytochrome concentrations obtained here and those obtained in the azo dye study [35], which are approximately 30% higher in all lactate:fumarate systems.

Finally, given that reaction rates between systems showed a trend, where higher reaction rate were observed for higher *c*-type cytochrome concentration, these systems are potentially good candidates for isotope analysis.

3.2 Effect of CymA and Fdh expressions on U(VI) reduction rates

Based on the results obtained in section 3.1.2, a further exploraton of the impact of specific *c*-type cytochromes on U(VI) reaction rates is warranted. Therefore, this section aims to understand the effect of over-expression of CymA and the enzyme Fdh (formate dehydrogenase) of *S. oneidensis*.

CymA is a *c*-type cytochrome associated with the inner membrane, acting as an essential corridor of respiratory electron transfer to the redox proteins located in the outer membrane [45]. Hence, the impact of over-expression of this gene on U(VI) reduction was investigated. Additionally, CymA over-expression was combined to *fdh* over-expression, the latter gene encodes Fdh protein, which oxidises formate, realising a pair of electrons [36]. This reaction, illustrated in Figure 1.1, is expected to enhance the electron transfer to CymA and ultimately might have an effect on U(VI) reduction rates. Finally, these two strains were compared to MR-1 wild type (WT) as a control.

As before, U(VI) reduction experiment were carried out using 5mM edta and the results are shown in Figure 3.7 and 3.8.

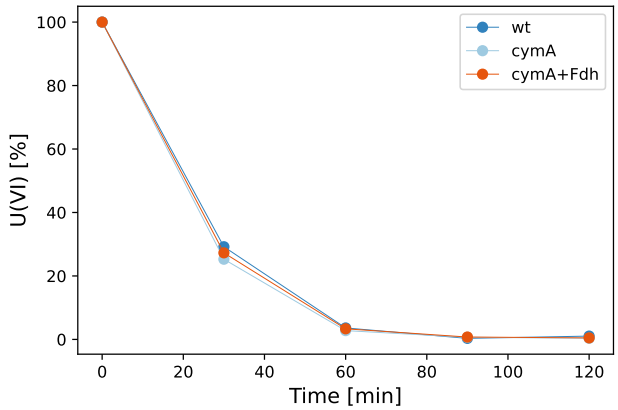

Figure 3.7: U(VI)-edta reduction over time for *S. oneidensis* wild-type, CymA and CymA+Fdh MR-1 recombinant. Results correspond to replicate A only.

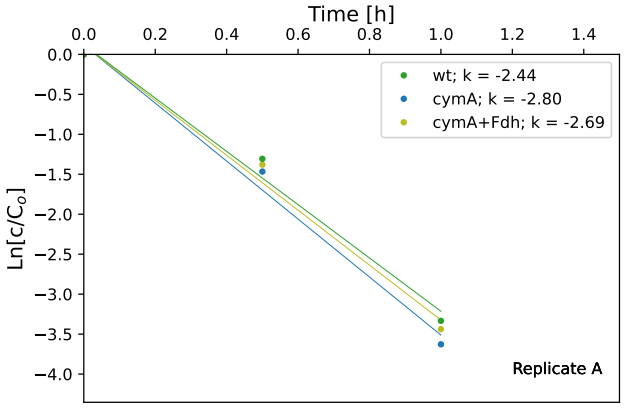

Figure 3.8: U(VI)-edta first order reduction rate by wild type, CymA and CymA+Fdh MR-1 recombinant. Linear fitting was made using the first three time-points corresponding to 97% reduction.

Figure 3.7 shows that the reaction reached completion after 60 min for all cases. However, no visible differences can be observed among different strains of MR-1, suggesting that over-expression of CymA and Fdh do not result in increases in U(VI) reduction rate. As this experiment showed markedly similar reduction rates for the three strains, these systems did not represent an opportunity to explore the impact of reduction rate on U isotope fractionation behavior. Hence, batch replicates were not performed.

Table 3.2: Normalized first order reaction rates (k) by total protein content for *S. oneidensis* wild-type, CymA and CymA+Fdh MR-1 recombinant.

Sample	$\boldsymbol{k}$ [h^{-1}mg $protein^{-1}$]
WT	-2.16
CymA	-2.03
CymA+Fdh	-1.95

In spite of a lack of replicates confirming these findings, a higher reduction rate would be expected for CymA over-expression, compared to the wild type. This is due to the fact that electrons are generated in the metabolism of lactate to be stored in form of NADH, then electrons are transferred subsequently from NADH to the inner membrane (IM) to cymA, which corresponds to the first conductive protein in the electron transport chain of *S. oneidensis*.[1]. Additionally, it has been reported in literature that cymA was successfully over-expressed, under aerobic and anaerobic conditions [45], suggesting that these results may not be due to a problem in the expression level of CymA, obtained during growth.

When over-expressing Fdh in combination with CymA, the reduction rate was expected to be further enhanced, however, this was also not the case. The possible explanation to this result might be related to the condition in which bacteria were grown. Authors have reported that formate, produced after lactate oxidation, is a key component for anaerobic growth of MR-1 and this latter compound is ultimately oxidized to CO_2 by Fdh protein, resulting in the generation of a pair of electrons that can be ultimately transferred downstream in the electron transport network. However, it has been reported that growing an Fdh strain in presence of oxygen, formate is not generated and growth is indistinguishable from MR-1 wild-type [36]. This statement allows us to suggest that, during the aerobic growth of the bacteria (i.e. before inoculation in the U(VI) containing reactor) formate may not have been generated and then during the anoxic reaction with uranium, formate was poorly generated given the low biomass in the reactor. Therefore, the results obtained for *cymA+fdh* recombinant in this experiment did not show a difference compared to wild type, since not sufficient formate was available for its oxidation by Fdh to further enhance the electron flux to CymA.

Similar edited MR-1 strains have been studied by Fan et al. (2021), in their work, CymA has been over-expressed together with MtrCAB and Fdh along with Mdh, showing enhanced U(VI) reduction rates in both cases [10]. From their work and our results it is possible to suggest that the greater reaction rates that they obtained may not be due to the presence of CymA or Fdh in those experiments but more probably due to the presence of MtrCAB and/or Mdh proteins.

Furthermore, there are two possible explanations for the obtained results in this experiment. Firstly, the edited MR-1 strains did not over-express the proteins CymA and Fdh despite the gene was encoded, hence, they behaved the same as wild type, however, this needs to be confirmed via RT-qPCR analysis. Secondly, these results suggest that CymA and Fdh are not the rate limiting step in the reaction and hence no differences were observed when comparing to wild-type.

3.3 Effect of MtrCAB expressions on U(VI) reduction rates

As addressed above, the mtr transmembrane complex has been shown to play an important role in U(VI) reduction. It is known that MR-1 facilitates electron transfer through the Mtr complex, where electrons are transferred from the periplasm to extracellular electron acceptors such as insoluble and soluble metals [46]. To investigate this further and to systematically impact the expression of the MtrCAB complex, the P_{BAD} promoter system was engineered into MR-1, in a similar approach to that by Fan et al., (2021) [10]. To this end, the impact of varying L-arabinose concentrations on the reduction rate of U(VI)-edta was explored.

First of all, in order to confirm to what extent L-arabinose concentrations impacted *mtrC* expression, RT-qPCR was performed and the results are illustrated in Figure 3.9.

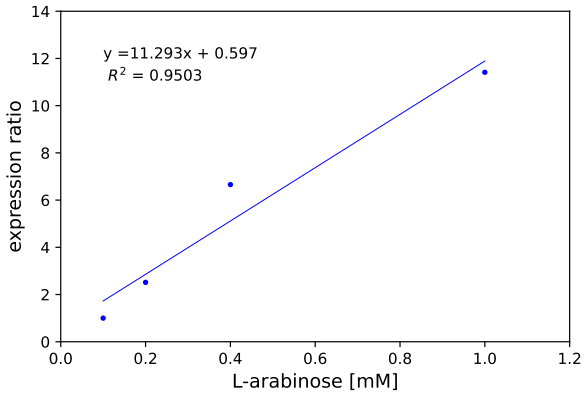

Figure 3.9: *mtrC* expression ratio obtained from RT-qPCR results (replicate A) in function of L-arabinose concentration. These results include four systems, corresponding to P_{BAD}-mtr strain grown in 0.1; 0.2; 0.4 and 1.0 mM of L-arabinose. Expression ratio is relative to 0.1 mM L-arabinose system.

Figure 3.9 illustrates that *mtrC* gene was systematically expressed as L-arabinose concen-

tration increased, suggesting that the concentration of MtrCAB complex was also increased. In fact, RT-qPCR results (Appendix F.2) showed that expression level obtained for 1 mM L-arabinose was 11.4-fold higher the expression level of 0.1 mM L-arabinose. Based on this result, it is expected that the successful modification of MtrCAB expression levels will have a significant effect on U(VI) reduction rates.

The following figures illustrate the results obtained for U(VI)-edta reduction over time and the first order reduction rates for the P_{BAD}-mtr MR-1 strain grown in four different L-arabinose concentrations.

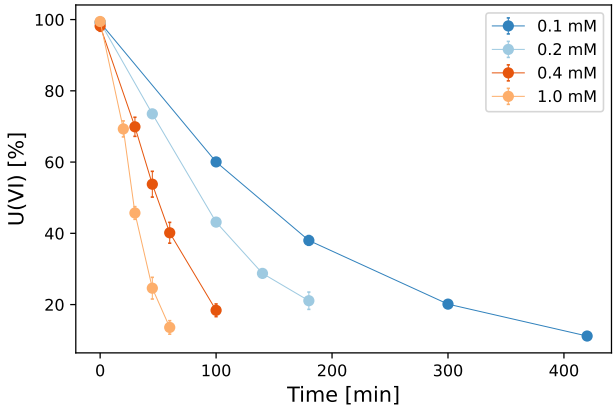

Figure 3.10: U(VI)-edta reduction over time for P_{BAD}-mtr MR-1 strain grown in 0.1; 0.2; 0.4 and 1.0 mM of L-arabinose. Results correspond to the mean of replicate A and B, where error bars represent 2σ.

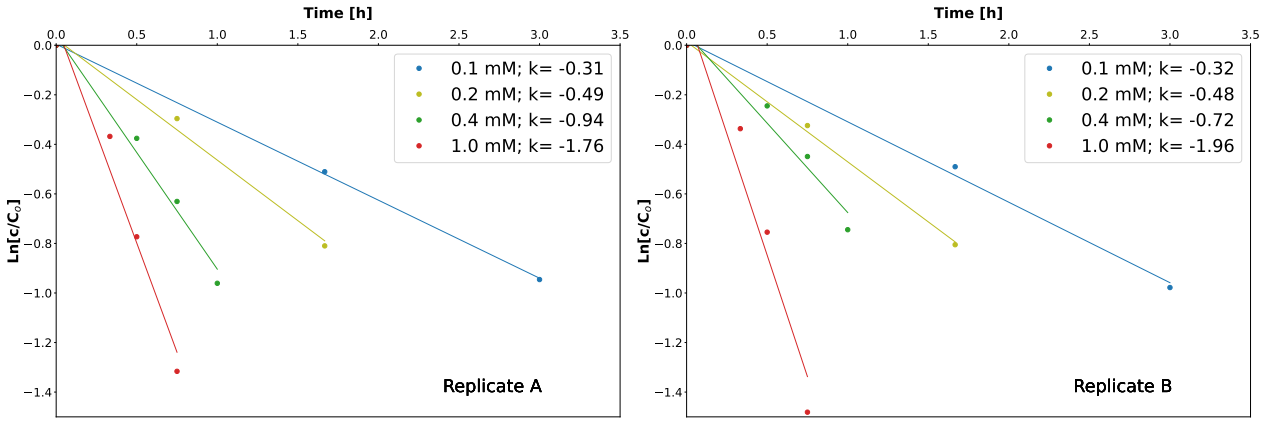

Figure 3.11: U(VI)-edta first order reaction rates for P_{BAD}-mtr MR-1 strain grown in 0.1; 0.2; 0.4 and 1.0 mM of L-arabinose. Linear fitting was made using the first three and four time-points for 0.1; 0.2 mM and 0.3; 0.4 mM L-arabinose systems respectively, corresponding to approximately 60% reduction for replicate A (left) and B (right).

Figure 3.10 shows that changing expression level of Mtr conductive complex affected dramatically the reduction capacity of *S. oneidensis*. In general, all strains reached around 90% of U(VI) removal, however, when using 1mM L-arabinose, this happened in only one hour. On the contrary, this same value was reached after seven hours when the same strain was grown in 0.1 mM L-arabinose.

Moreover, the reaction rate obtained for different L-arabinose concentrations are shown in Figure 3.11. This figure illustrates that Mtr expression level affects dramatically the reaction rate in both replicate. The normalized values of first order reaction rate are reported in Table 3.3 and confirm this effect, showing a systematic increase of reaction rate when L-arabinose was increased. In fact, when comparing two extreme L-arabinose concentrations systems, 1 mM was 6.7-fold faster compared to 0.1 mM system.

Table 3.3: Normalized first order reaction rates (k) by total protein content for four different systems with different L-arabinose concentration. A and B represent replicate results.

	$\boldsymbol{k}$ [h^{-1}mg protein^{-1}]			
Sample	**A**	**B**	**mean**	**SD (σ)**
0.1 mM L-arabinose	-1.84	-1.87	-1.86	0.02
0.2 mM L-arabinose	-4.30	-2.61	-3.46	1.20
0.4 mM L-arabinose	-7.48	-5.03	-6.25	1.73
1.0 mM L-arabinose	-15.54	-9.29	-12.42	4.42

The effect of expression level on U(VI) reduction rate is clearly illustrated in Figure 3.12, showing that there is a linear relationship between U(VI) reaction rate and expression ratio. These result confirm the previous suggestion, that increases in *mtrC* expression results in increases in the MtrCAB concentration. In this manner, this result suggest that the reaction rate is determined by the amount of MtrCAB, in agreement with previous findings [10].

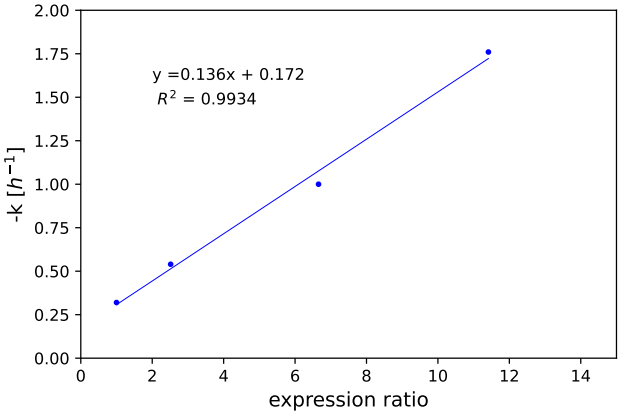

Figure 3.12: First order reaction rate constants (k) in function of expression level ratio of *mtrC* (replicate A). Ratio is relative to 0.1 mM L-arabinose system.

Additionally, given that MtrC is located on the outer membrane, exposed to the surface, these data also suggest that reduction of U(VI)-edta occurs mainly extra-cellularly. The latter has been reported by authors working with MR-1 strains, lacking MtrC and/or omcA during U(VI)-carbonate reduction [27]. In this study, they demonstrated that Mtr respiratory pathway is essential for the reduction reaction and also that decaheme cytochromes located in the OM (MtrC and OmcA) are required for the majority of this activity. They also reported that UO_2 nanoparticles products accumulated in suspension extracellurlarly and most of them were in complex form with extracellular polymeric substance (EPS). However, this does not rule out the possibility that other reductases are used by MR-1 when outer membrane *c*-type cytochromes expression is fully suppressed.

3.4 Impact of reaction rates on uranium fractionation

To determine the impact of U(VI) reduction rates on isotope fractionation, and to attempt to mechanistically relate U(VI) reduction rates to observed isotope fractionation factors, isotope signatures from reactions containing MR-1 with different expression levels of the Mtr complex were measured. To this end, U(VI) fractions at time-points throughout the reactions of systems containing the MR-1 strains grown with either 0.1 or 1 mM L-arabinose were analyzed, as these systems displayed the greatest difference in reaction rate, as was shown in Section 3.3.

Figure 3.13-A shows ^{238}U isotope signature obtained for both systems studied. Here, $\delta^{238}U$ is moving towards negative values, which indicate the preferential incorporation of ^{238}U into the reduced form U(IV), in agreement with results reported in other studies [9][18].

In the same line, a previous study using uranyl carbonate as a substrate demonstrated that higher fractionation is observed for slower U(VI) reaction rates [8]. Figure 3.13-B illustrates the fitted Rayleigh models for both L-arabinose systems, whilst a single model for each case would be conventional, an initial model fitting all data points led to a non-expected relationship between U(VI) reaction rate and isotope fractionation (Appendix G.1) respect to those results reported by Basu et al.,(2020).

This initial model showed lower fractionation for the system 0.1 mM L-arabinose and only reached an R^2 of 0.95. In the case of 1.0 mM, results showed better fit with R^2 of 0.98 (Appendix G.1). In the same line, the fit of the Rayleigh distillation in this first model showed that the y-axis of both systems do not intersect the value of the initial stock concentration. Based on this, it was decided to fit the 0.1 mM L-arabinose system using the first three data points, which increased R^2 up to 0.99, and allowed to intersect the y-axis of both systems together as it is shown in Figure 3.13-B. Moreover, with these models, enrichment factors (ε) of 1.05‰ and 0.88 ‰ were obtained for 0.1 mM and 1.0 mM L- arabinose respectively, showing that, as expected, higher isotopic fractionation is observed for slower U(VI) reduction rate [8].

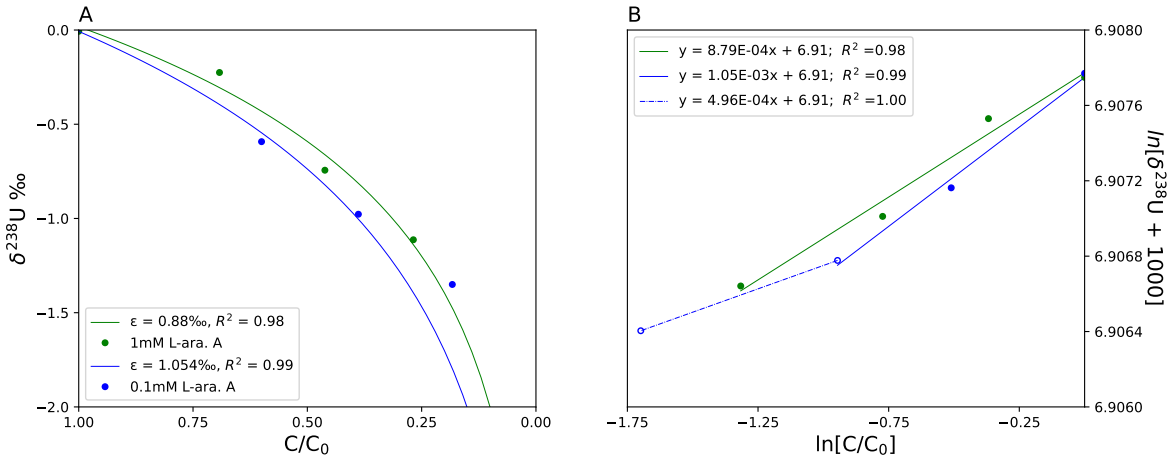

Figure 3.13: Isotope fractionation results obtained for P_{BAD}-mtrCAB MR-1 strain grown in 0.1 and 1.0 mM L-arabinose (replicate A only). Panel (A) illustrates $\delta^{238}U$ values against unreacted fraction of U(VI), where ε values are reported. Panel (B) shows the Rayleigh distillation model fit for both systems. Note that models were fitted using three and four data points for 0.1 and 1.0 mM L-arabinose systems, respectively.

The reasoning of fitting two models for the same system is explained using two end member scenarios as an example. Figure 3.14 illustrate two cases, on one hand, case A corresponds to a system with high reaction rate, hence fast enzymatic reaction. Here, the uranium concentration is low relative to the amount of MtrC available and, as lactate is not limiting, the hemes of MtrC are fully reduced. Therefore, given the high electron flux from MtrC and as U(VI) atoms are distributed among a higher concentration of MtrC, the reaction is unidirectional (i.e. U(VI) reduction is quantitative), such that the available ^{235}U(VI) and ^{238}U(VI) concentration quickly approach concentration values near to zero. Consequently, only a minor discrimination between uranium isotopes occurs, represented by a small slope in the case A model of Figure 3.14.

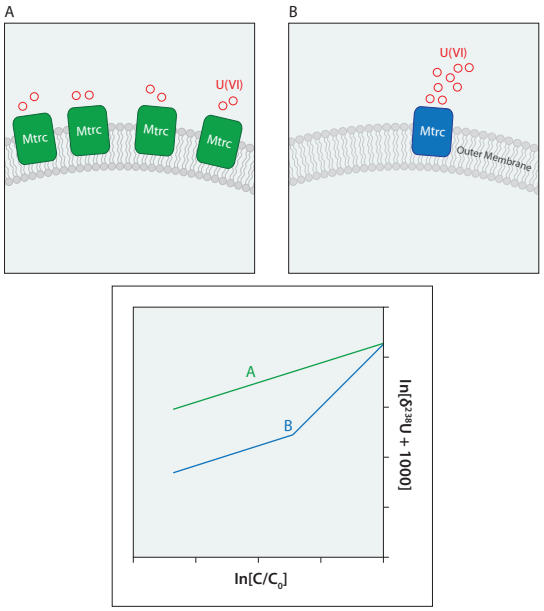

Figure 3.14: Schematic illustration of two extreme end members scenario: Case A represents a fast reaction rate due to higher expression level of MtrC; Case B corresponds to a slow reaction rate represented by low MtrC concentration. The linear relationship between $ln[\delta^{238}U + 1000]$ in function of $ln[C/C_0]$ for two end member denotes the fractionation magnitude.

On the other hand, case B illustrates a slow enzymatic reaction system, where U(VI) concentration is relatively higher with respect to the available amount of MtrC. In this case, U(VI) has to wait to get reduced, meaning that the faster reaction rates for ^{238}U (as a result of their greater stability in the U(IV) product), lead to the preferential reaction of ^{238}U and hence, more observable fractionation, represented by a large slope in the Rayleigh model of Figure 3.14.

These scenarios are consistent with a recently published steady-state model of uranium

reduction and fractionation [47], which indicates that very uni-directional reactions (such as those where U supply is rate limiting) would result in limited fractionation.

It is, therefore, intuitive that systems showing case B behaviour, will transition to case A behaviour once U(VI) concentrations become low enough as the reduction reaction progresses. When this happens, reduction becomes quantitative and fractionation will decrease. Hence, the slope of the Rayleigh model would be expected to shift toward a similar magnitude as that in case A.

Here, the fractionation data obtained for the two systems with different expression levels of *mtrC* appear to fit within these two end member scenarios. First, the 1 mM L-arabinose system, with high *mtrC* expression levels showed the lowest fractionation, described with a single Rayleigh model, as in case A (Figure 3.13-A). On the other hand, the 0.1 mM L-arabinose system, with lower levels of *mtrC* expression, shows more fractionation in the initial reaction stages ($\varepsilon_{caseB} > \varepsilon_{caseA}$), followed by a transition to a case A type Rayleigh model (with lower fractionation) as the reaction progresses ($\varepsilon_{B,phase1}) > \varepsilon_{B,phase2}$).

Similar findings have been reported by other authors working on U(VI) fractionation during biotic reduction [8]. In their work, they have shown that at higher initial U(VI) concentrations (i.e. where U(VI) concentrations are high with respect to *c*-type cytochromes) isotopic fractionation was higher. Conversely, at lower initial U(VI) concentrations, isotopic fractionation was significant lower. In this study, the authors considered a conceptual model where cells were surrounded by boundary layers with U(VI) concentrations lower than in the bulk solution, based on this idea, they assumed that the reaction occurs in two steps: (i) the diffusive transport of the U(VI) substrate through the boundary layers and (ii) the enzymatic U(VI) reduction at the surface or periplasm of the cell [8].

Despite the trend in our results followed the same behavior as the study mentioned [8], it is difficult to reconcile their findings with the data presented here given that our study have only impacted reduction rates by changing MtrC concentrations and not U(VI) concentrations. However, taken together, these data collectively suggest that it is the relationship between U(VI) supply and reduced MtrC content that are important in the uranium fractionation during its biotic reduction.

It is important to note that the results shown in this section correspond to data from one biological replicate only. Additionally, the fitting of a second model in the 0.1 mM L-arabinose system was made using only two points. However, the application of a second, smaller coefficient Rayleigh model in the later stages of reduction may be justified given that similar anomalously heavy values at late-stage reduction have been seen before. Here, the

authors suggested that these data points corresponded to contamination of U(VI) samples with heavy U(IV) products and so were excluded from their analysis [8]. This similar trend in both data suggest that this phenomena may indeed be due to the relative availability of the U(VI) substrate with respect to the number of *c*-type cytochromes available for the reaction.

Clearly, it is essential to obtain more data from late time-points in order to confirm whether there is a transition point at which U(VI) reduction moves towards a quantitative, unidirectional reaction displaying limited fractionation. Furthermore, obtaining isotope signatures from the remaining systems with 0.2 and 0.4 mM L-arabinose-grown cells would provide further evidence of any systematic relationship between substrate and MtrC availability and ultimately, its effect on fractionation.

Finally, based on these results, it is possible to confirm that U(VI) reaction rate impacts uranium fractionation, however, reaction rate does not control fractionation on its own and this phenomena is also governed by others factors, such as, the ratio of substrate and reduced *c*-type cytochromes available.

Chapter 4

Conclusion

The present study aimed at understanding the impact of U(VI) reduction rate on isotopic fractionation. To this end, modification of key components of the electron transport network of *S. oneidensis* MR-1 on U(VI) reduction was explored. In order to address this, we investigated two different aspects and their impact on U(VI) reduction rate: (1) The impact of varying electron donor-acceptor ratios on *c*-type cytochrome concentration and (2) The impact of varying expression levels of targeted key proteins in the electron transfer network of *S. oneidensis*. Subsequently, this allowed us to effectively modify U(VI) reaction rate to assess its impact on uranium fractionation.

The results presented in this study confirmed the relationship between the availability of electron acceptor and *c*-type cytochrome concentration in *S. oneidensis*. The data showed here was consistent with previous findings [35], showing that fumarate (electron acceptor) limited media favored *c*-type cytochrome expression. Additionally, by varying the global concentration of *c*-type cytochromes via different electron donor-acceptor ratios, U(VI) reaction rates can be moderately impacted. However, the magnitude of this impact was smaller compared to that reported for azo dye reduction rates [35].

On the other hand, the study of over-expression of CymA and Fdh during U(VI) reduction showed that these two proteins are not a rate limiting factor in *S. oneidensis* under the conditions tested here. However, expression levels analysis is needed to determine whether this conclusion is correct.

Additionally, in this study was also demonstrated that U(VI) reduction rate is strongly impacted by MtrCAB expression levels, and that an engineered system using P_{BAD}-mtr promoter in different L-arabinose concentrations allowed us to systematically impact this expression and therefore, U(VI) reaction rate. Based on these results and in agreement with

the literature [10] it was determined that the MtrCAB complex plays a key role in the electron transport network of *S. oneidensis* during U(VI) reduction.

The systematic modification of U(VI) reaction rates displayed using the P_{BAD}-mtr promoter system provided the adequate conditions for isotope analysis. The results obtained showed that isotopic fractionation of uranium is impacted by reaction rate and higher fractionation was observed for slower reactions, but this relationship appears to be governed by the relative availability of substrate with respect to MtrC present rather than reaction rate itself.

The results presented here contribute toward an improved understanding of the factors that determine isotopic fractionation during enzymatic reduction of U(VI). In this manner, uranium isotopes may be a suitable redox proxy to monitoring U(VI) reduction during remediation studies [9]. Moreover, knowing that substrate concentration impacts fractionation, the environmental conditions that affect U(VI) concentrations need to be taken into account in bioremediation studies. In this sense, U(VI) concentration in the environment can be affected by other processes apart from bio-reduction, such as biomineralization, biosorption, abiotic reduction, among others [16][9], which may potentiality impact fractionation results.

Moreover, in this study we opted to study U(VI)-edta complex, however, for bioremediation proposes, uranium needs to be reduced to a precipitated form. In this sense, it is reported that U(VI) is mostly present in nature as a complex with carbonate, forming a precipitate after its reduction [27], which could ultimately impact uranium fractionation in a different manner as the one observed here. Additionally, these results corresponded to no-limited lactate conditions, however, in natural environments the carbon source availability may vary, affecting electron flux and more likely uranium fractionation behaviour. Therefore, it is important to highlight that the results reported in this study are valid under the specific laboratory conditions detailed here, different to the case in natural environments, where uranium speciation and carbon source concentration may impact reduction rates and thereby, fractionation.

Although progress has been made in understanding uranium fractionation during bioreduction, there is still a paucity of data to mechanistically relate these two variables. Thus, the future direction of this study should seek to confirm that under very fast reaction conditions, fractionation would be minuscule. The latter could be done by testing the pure protein MtrC under the same conditions and it would be expected that this will increase reaction rate and ultimately, show insignificant fractionation, since the ratio between (VI) and MtrC hemes fully reduced would be considerably smaller, leading to a fast and quantitative reaction.

In the same line, this study lacked the analysis under electron donor limited conditions. Hence, it is necessary to perform same experiment but varying lactate concentrations, since it is very likely that under severe limited conditions, fractionation will not be impacted in the same manner and higher fractionation may be observed for high MtrC expression level. This is due to the impact caused on the electron flux from each MtrC, which would be smaller for higher MtrC concentrations under lactate limited conditions. Thus, decreasing electron flux, when more MtrC are present, will imply that less sites in the MtrC hemes are reduced and therefore, the back reaction would be more likely to occur, which may lead to the preferential reduction of the heavier isotope and consequently, higher fractionation.

Moreover, the lactate:fumarate systems obtained in this study are potentially good candidates for isotopic fractionation analysis. In this sense, it would interesting to compare the fumarate limited system (L100F20) to wild-type grown aerobically in LB. This would give insights of the general impact caused by *c*-type cytochromes on uranium fractionation.

Finally, it would be interesting to study how electron flux is impacted by varying the global *c*-type cytochrome concentration and how this ultimately impacts uranium fractionation. To this end, the EET ability of *S. oneidensis* grown in different lactate:fumarate ratios could be evaluated by microbial electrolysis cell assay (MEC). This experiment will provide current density results for each system and would give the possibility of finding a quantifiable relationship between electron flux and isotopic fractionation. Then, this information could be complemented with RT-qPCR of targeted proteins to further comprehend what *c*-type cytochromes were involved during the anaerobic growth of *S. oneidensis*.

Bibliography

[1] Judy D Wall and Lee R Krumholz. Uranium Reduction. *Annual Review of Microbiology*, 60:149–166, 2006.

[2] Margaux Molinas, Radmila Faizova, Ashley Brown, Jurij Galanzew, Bianca Schacherl, Barbora Bartova, Karin L. Meibom, Tonya Vitova, Marinella Mazzanti, and Rizlan Bernier-Latmani. Biological Reduction of a U(V)-Organic Ligand Complex. *Environmental Science and Technology*, 55(8):4753–4761, 4 2021.

[3] Daniel S. Alessi, Juan S. Lezama-Pacheco, Joanne E. Stubbs, Markus Janousch, John R. Bargar, Per Persson, and Rizlan Bernier-Latmani. The product of microbial uranium reduction includes multiple species with U(IV)-phosphate coordination. *Geochimica et Cosmochimica Acta*, 131:115–127, 2014.

[4] Rizlan Bernier-Latmani, Harish Veeramani, Elena Dalla Vecchia, Pilar Junier, Juan S. Lezama-Pacheco, Elena I. Suvorova, Jonathan O. Sharp, Nicholas S. Wigginton, and John R. Bargar. Non-uraninite products of microbial U(VI) reduction. *Environmental Science and Technology*, 44(24):9456–9462, 12 2010.

[5] Claudine H. Stirling, Morten B. Andersen, Rolf Warthmann, and Alex N. Halliday. Isotope fractionation of 238U and 235U during biologically-mediated uranium reduction. *Geochimica et Cosmochimica Acta*, 163:200–218, 2015.

[6] Sebastian Beblawy, Thea Bursac, Catarina Paquete, Ricardo Louro, Thomas A. Clarke, and Johannes Gescher. Extracellular reduction of solid electron acceptors by Shewanella oneidensis. *Molecular Microbiology*, 109(5):571–583, 9 2018.

[7] Atsushi Kouzuma, Takuya Kasai, Atsumi Hirose, and Kazuya Watanabe. Catabolic and regulatory systems in shewanella oneidensis MR-1 involved in electricity generation in microbial fuel cells. *Frontiers in Microbiology*, 6(JUN):609, 2015.

[8] Anirban Basu, Christoph Wanner, Thomas M. Johnson, Craig Lundstrom, Robert A Sanford, Eric Sonnenthal, Maxim I. Boyanov, and Kenneth M. Kemner. Microbial

U isotope fractionation depends on U(VI) reduction rate. *Environmental Science & Technology*, (Vi), 2020.

[9] Malgorzata Stylo, Nadja Neubert, Yuheng Wang, Nikhil Monga, Stephen J. Romaniello, Stefan Weyer, and Rizlan Bernier-Latmani. Uranium isotopes fingerprint biotic reduction. *Proceedings of the National Academy of Sciences of the United States of America*, 112(18):5619–5624, 2015.

[10] Yang-Yang Fan, Qiang Tang, Feng-He Li, Hong Sun, Di Min, Jing-Hang Wu, Yang Li, Wen-Wei Li, and Han-Qing Yu. Enhanced Bioreduction of Radionuclides by Driving Microbial Extracellular Electron Pumping with an Engineered CRISPR Platform. *Environmental Science & Technology*, 2021.

[11] Marcus J. Edwards, Gaye F. White, Julea N. Butt, David J. Richardson, and Thomas A. Clarke. The Crystal Structure of a Biological Insulated Transmembrane Molecular Wire. *Cell*, 181(3):665–673, 4 2020.

[12] F. Saida, M. Uzan, B. Odaert, and F. Bontems. Expression of Highly Toxic Genes in E. coli: Special Strategies and Genetic Tools. *Current Protein and Peptide Science*, 7(1):47–56, 2006.

[13] Uday Kumar Banala, Nilamadhab Prasad Indradyumna Das, and Subba Rao Toleti. Microbial interactions with uranium: Towards an effective bioremediation approach. *Environmental Technology & Innovation*, 21:101254, 2 2021.

[14] Aino Maija Lakaniemi, Grant B. Douglas, and Anna H. Kaksonen. Engineering and kinetic aspects of bacterial uranium reduction for the remediation of uranium contaminated environments. *Journal of Hazardous Materials*, 371(January):198–212, 2019.

[15] Kenneth H. Williams, John R. Bargar, Jonathan R. Lloyd, and Derek R. Lovley. Bioremediation of uranium-contaminated groundwater: A systems approach to subsurface biogeochemistry. *Current Opinion in Biotechnology*, 24(3):489–497, 2013.

[16] Laura Newsome, Katherine Morris, and Jonathan R. Lloyd. The biogeochemistry and bioremediation of uranium and other priority radionuclides. *Chemical Geology*, 363:164–184, 1 2014.

[17] Manish Tiwari, Ashutosh K. Singh, and Devesh K. Sinha. Stable Isotopes: Tools for Understanding Past Climatic Conditions and Their Applications in Chemostratigraphy. In *Chemostratigraphy: Concepts, Techniques, and Applications*, pages 65–92. Elsevier, 1 2015.

[18] Yvonne Roebbert, Chris Daniel Rosendahl, Ashley Brown, Axel Schippers, Rizlan Bernier-Latmani, and Stefan Weyer. Uranium isotope fractionation during the anoxic mobilization of noncrystalline U(IV) by ligand complexation. *Environmental Science and Technology*, 55(12):7959–7969, 6 2021.

[19] Jacob Bigeleisen. Nuclear size and shape effects in chemical reactions. Isotope chemistry of the heavy elements. *Journal of the American Chemical Society*, 118(15):3676–3680, 4 1996.

[20] Sha Yang and Yun Liu. Nuclear field shift effects on stable isotope fractionation: a review. *Acta Geochimica*, 35(3):227–239, 9 2016.

[21] S. Weyer, A. D. Anbar, A. Gerdes, G. W. Gordon, T. J. Algeo, and E. A. Boyle. Natural fractionation of 238U/235U. *Geochimica et Cosmochimica Acta*, 72(2):345–359, 2008.

[22] Claudine H. Stirling, Morten B. Andersen, Emma Kate Potter, and Alex N. Halliday. Low-temperature isotopic fractionation of uranium. *Earth and Planetary Science Letters*, 264(1-2):208–225, 2007.

[23] Geoffrey J. Gilleaudeau, Stephen J. Romaniello, Genming Luo, Alan J. Kaufman, Feifei Zhang, Robert M. Klaebe, Linda C. Kah, Karem Azmy, Julie K. Bartley, Wang Zheng, Andrew H. Knoll, and Ariel D. Anbar. Uranium isotope evidence for limited euxinia in mid-Proterozoic oceans. *Earth and Planetary Science Letters*, 521:150–157, 2019.

[24] Xinze Lu, Tais W. Dahl, Wang Zheng, Su Wang, and Brian Kendall. Estimating ancient seawater isotope compositions and global ocean redox conditions by coupling the molybdenum and uranium isotope systems of euxinic organic-rich mudrocks. *Geochimica et Cosmochimica Acta*, 290:76–103, 2020.

[25] Charles John Bopp, Craig C. Lundstrom, Thomas M. Johnson, Robert A. Sanford, Philip E. Long, and Kenneth H. Williams. Uranium 238U/235U Isotope Ratios as Indicators of Reduction: Results from an in situ Biostimulation Experiment at Rifle, Colorado, U.S.A. *Environmental Science and Technology*, 44(15):5927–5933, 8 2010.

[26] Alyssa E. Shiel, Parker G. Laubach, Thomas M. Johnson, Craig C. Lundstrom, Philip E. Long, and Kenneth H. Williams. No measurable changes in 238U/235U due to desorption-adsorption of U(VI) from groundwater at the Rifle, Colorado, integrated field research challenge site. *Environmental Science and Technology*, 47(6):2535–2541, 2013.

[27] Matthew J. Marshall, Alexander S. Beliaev, Alice C. Dohnalkova, David W. Kennedy, Liang Shi, Zheming Wang, Maxim I. Boyanov, Barry Lai, Kenneth M. Kemner, Jeffrey S. McLean, Samantha B. Reed, David E. Culley, Vanessa L. Bailey, Cody J. Simonson, Daad A. Saffarini, Margaret F. Romine, John M. Zachara, and James K. Fredrickson. c-type cytochrome-dependent formation of U(IV) nanoparticles by Shewanella oneidensis. *PLoS Biology*, 4(8):1324–1333, 2006.

[28] Terry E. Meyer, Alexandre I. Tsapin, Isabel Vandenberghe, Lina De Smet, Dmitrij Frishman, Kenneth H. Nealson, Michael A. Cusanovich, and Jozef J. Van Beeumen. Identification of 42 Possible Cytochrome C Genes in the Shewanella oneidensis Genome and Characterization of Six Soluble Cytochromes. *OMICS A Journal of Integrative Biology*, 8(1):57–77, 2004.

[29] Shenghua Jiang and Hor Gil Hur. Effects of the anaerobic respiration of Shewanella oneidensis MR-1 on the stability of extracellular U(VI) nanofibers. *Microbes and Environments*, 28(3):312–315, 2013.

[30] Dan Coursolle, Daniel B. Baron, Daniel R. Bond, and Jeffrey A. Gralnick. The Mtr respiratory pathway is essential for reducing flavins and electrodes in Shewanella oneidensis. *Journal of Bacteriology*, 192(2):467–474, 2010.

[31] Feng Li, Yuanxiu Li, Liming Sun, Xiaoli Chen, Xingjuan An, Changji Yin, Yingxiu Cao, Hui Wu, and Hao Song. Modular Engineering Intracellular NADH Regeneration Boosts Extracellular Electron Transfer of Shewanella oneidensis MR-1. 2018.

[32] Erica L.-W. Majumder and Judy D. Wall. Uranium Bio-Transformations: Chemical or Biological Processes? *Open Journal of Inorganic Chemistry*, 07(02):28–60, 2017.

[33] Joanna C. Renshaw, Laura J.C. Butchins, Francis R. Livens, Iain May, John M. Charnock, and Jonathan R. Lloyd. Bioreduction of uranium: Environmental implications of a pentavalent intermediate. *Environmental Science and Technology*, 39(15):5657–5660, 2005.

[34] José M. Cerrato, Matthew N. Ashner, Daniel S. Alessi, Juan S. Lezama-Pacheco, Rizlan Bernier-Latmani, John R. Bargar, and Daniel E. Giammar. Relative reactivity of biogenic and chemogenic uraninite and biogenic noncrystalline U(IV). *Environmental Science and Technology*, 47(17):9756–9763, 2013.

[35] Hui Wang, Elon Correa, Warwick B. Dunn, Catherine L. Winder, Royston Goodacre, and Jonathan R. Lloyd. Metabolomic analyses show that electron donor and ac-

ceptor ratios control anaerobic electron transfer pathways in Shewanella oneidensis. *Metabolomics*, 9(3):642–656, 12 2013.

[36] Aunica L. Kane, Evan D. Brutinel, Heena Joo, Rebecca Maysonet, Chelsey M. VanDrisse, Nicholas J. Kotloski, and Jeffrey A. Gralnick. Formate metabolism in Shewanella oneidensis generates proton motive force and prevents growth without an electron acceptor. *Journal of Bacteriology*, 198(8):1337–1346, 2016.

[37] A Berry Andbernardl Trumpower. Simultaneous determination of hemes a, b, and c from pyridine hemochrome spectra. *Analytical Biochemistry*, 15(1):1–15, 2003.

[38] Thermo Fisher Scientific Inc. Protein Assay Technical Handbook. *Thermo Scientific Pierce*, page 42, 2010.

[39] Deborah L Stoliker, Nazila Kaviani, Douglas B Kent, and James A Davis. Evaluating ion exchange resin efficiency and oxidative capacity for the separation of uranium(IV) and uranium(VI). *Geochemical Transactions*, 14(1):1, 2013.

[40] Eleni Maragkou and Ioannis Pashalidis. Investigations on the Interaction of EDTA with Calcium Silicate Hydrate and Its Impact on the U(VI) Sorption. *Coatings 2021, Vol. 11, Page 1037*, 11(9):1037, 8 2021.

[41] Sooyeon Kim, Will M. Bender, and Udo Becker. Exploring the kinetics of actinyl–EDTA reduction by ferrous iron using quantum-mechanical calculations. *Physical Chemistry Chemical Physics*, 23(9):5298–5314, 3 2021.

[42] Ling Sheng, Jennifer Szymanowski, and Jeremy B. Fein. The effects of uranium speciation on the rate of U(VI) reduction by Shewanella oneidensis MR-1. *Geochimica et Cosmochimica Acta*, 75(12):3558–3567, 6 2011.

[43] Liang Shi, Baowei Chen, Zheming Wang, Dwayne A. Elias, M. Uljana Mayer, Yuri A. Gorby, Shuison Ni, Brian H. Lower, David W. Kennedy, David S. Wunschel, Heather M. Mottaz, Matthew J. Marshall, Eric A. Hill, Alexander S. Beliaev, John M. Zachara, James K. Fredrickson, and Thomas C. Squier. Isolation of a high-affinity functional protein complex between OmcA and MtrC: Two outer membrane decaheme c-type cytochromes of Shewanella oneidensis MR-1. *Journal of Bacteriology*, 188(13):4705–4714, 7 2006.

[44] Michael Kudlich, Andreas Keck, Joachim Klein, and Andreas Stolz. Localization of the enzyme system involved in anaerobic reduction of azo dyes by Sphingomonas sp. Strain

BN6 and effect of artificial redox mediators on the rate of azo dye reduction. *Applied and Environmental Microbiology*, 63(9):3691–3694, 1997.

[45] Aswini Vellingiri, Young Eun Song, Ganapathiraman Munussami, Changman Kim, Chulhwan Park, Byong Hun Jeon, Sun Gu Lee, and Jung Rae Kim. Overexpression of c-type cytochrome, CymA in Shewanella oneidensis MR-1 for enhanced bioelectricity generation and cell growth in a microbial fuel cell. *Journal of Chemical Technology and Biotechnology*, 94(7):2115–2122, 7 2019.

[46] Dan Coursolle and Jeffrey A Gralnick. Modularity of the Mtr respiratory pathway of Shewanella oneidensis strain MR-1m mi_7266 995..1008. 2010.

[47] Ataru Sato, Rizlan Bernier-Latmani, Masahiko Hada, and Minori Abe. Ab initio and steady-state models for uranium isotope fractionation in multi-step biotic and abiotic reduction. *Geochimica et Cosmochimica Acta*, 2021.

Appendix A

Washing medium solutions preparation

A.1 PIPES-bicarbonate medium

500 mL of PIPES-bicarbonate medium were prepared for each experiment. The solution containing 20 mM of PIPES were stirred and pH was adjusted to 6.8 using 0.1 and 10 M NaOH solution. The solution was filter-sterilized into a sterile bottle and was purge with N_2 for 1 hour.

1M bicarbonate was prepared separately. First, bicarbonate was weight into a 30 mL serum bottle and moved to the anoxic chamber and then MiliQ water was added to prepare solution. Finally, 30 mL of the 1M bicarbonate solution was added, in the anoxic chamber, to the PIPES washing medium.

A.2 PIPES-edta and PIPES-edta-lactate medium

250 mL of PIPES-edta medium was prepared for each experiment. The solution contained 20 mM pipes and 5 mM of edta was stirred and pH was adjusted to 7.1 using 0.1 and 10 M NaOH solution.

30 mL of the previous solution were set apart and sodium-lactate was added to reach a concentration of 20 mM. The solution was transferred to a 30 mL serum bottle and sterilized in autoclave.

The remaining 220 mL of PIPES-edta medium were filter-sterilized into a sterile bottle and was purge with N_2 for 1 hour.

Appendix B

Summary of results

B.1 Normalized first order reaction rates obtained in each experiment

Table B.1: summary of normalized first order reaction rates (k) by protein content for variable obtained for each experiment

		k [h^{-1}mg protein^{-1}]			
Experiment	**System**	**A**	**B**	**mean**	**SD (σ)**
Variable c-type cytochrome concentration	L20F100	-108.8	-102.6	-105.7	4.3
	L50F50	-160.3	-108.8	-134.6	36.4
	L100F20	-155.8	-168.3	-162.1	8.8
CymA and CymA+Fdh MR-1 recombinant	Wild-type	-2.16	-	-	-
	CymA	-2.03	-	-	-
	Cym+Fdh	-1.95	-	-	-
P_{BAD}-MtrCAB promoter	0.1 mM L-arabinose	-1.84	-1.87	-1.86	0.02
	0.2 mM L-arabinose	-4.30	-2.61	-3.46	1.20
	0.4 mM L-arabinose	-7.48	-5.03	-6,.5	1.73
	1.0 mM L-arabinose	-15.54	-9.29	-12.42	4,42

Appendix C

Chemical speciation of uranium

C.1 Uranyl chemical speciation models

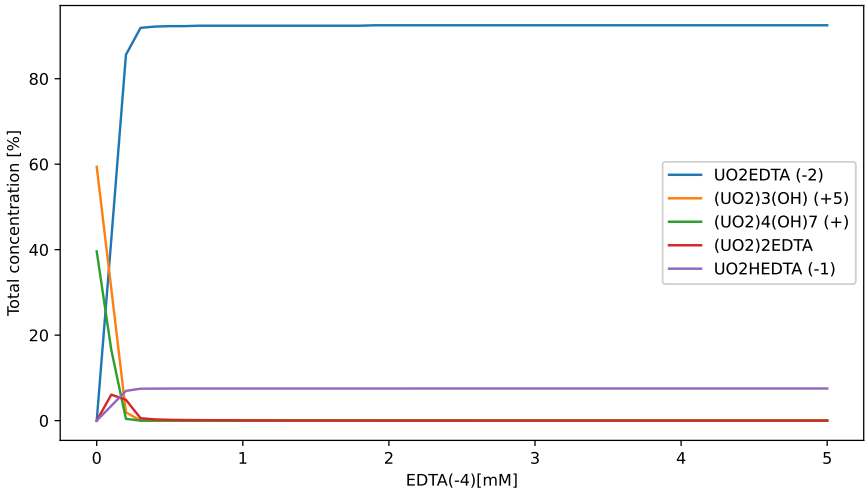

Figure C.1: MINEQL+ model of U(VI)-edta speciation at different edta concentrations under the following conditions: 200uM U(VI), 5 mM edta.

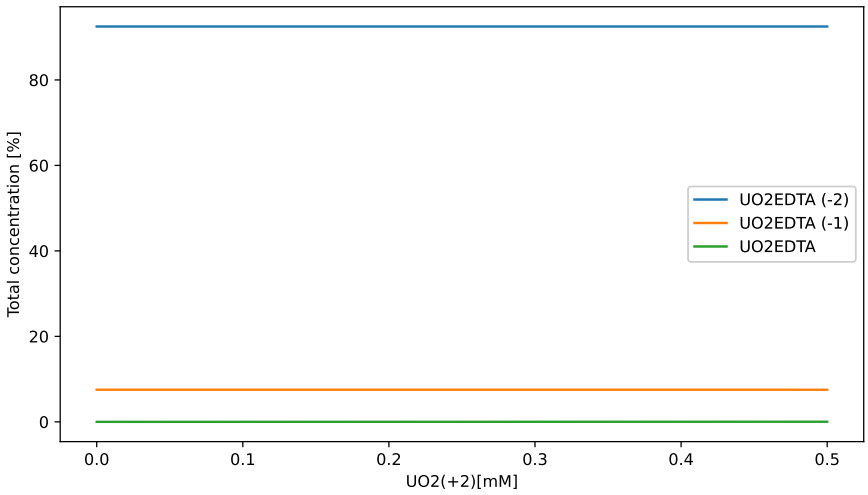

Figure C.2: MINEQL+ model of U(VI)-edta speciation at different Uranyl(VI) concentrations under the following conditions: 200uM U(VI), 5 mM edta.

Appendix D

Variable *c*-type cytochrome concentration experiment

D.1 Anaerobic growth of *S. oneidensis* for different lactate:fumarate ratios

Figure D.1: Samples of different Lactate:Fumarate ratios after 48 hours growth, where pink color was obtained for fumarate limited system. Note that for the sample Lactate 100 mM: Fumarate 20 mM, this color is less intense due to the lower biomass produced compared to the other two cases.

D.2 Spectra of pyridine hemochromes analysis

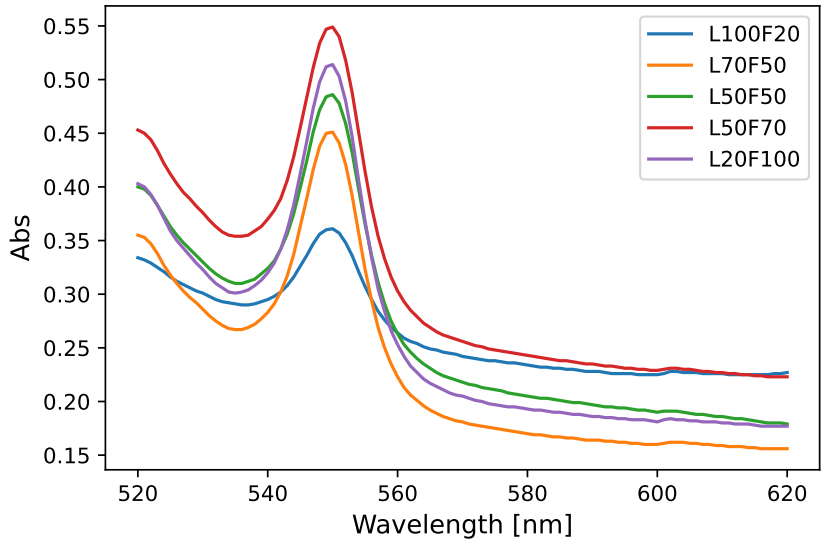

Figure D.2: Comparison of Pyridine hemochrome reduced spectra for five samples with different electron donor-acceptor ratios. Numbers in the notation represent mM of lactate and fumarate, respectively. Characteristic signal was obtained at 550 nm for every system.

D.3 *C*-type cytochrome concentrations obtained for samples with different electron donor-acceptor ratios

Table D.1: c-type cytochrome concentration normalized by total protein content, for different lactate-fumarate systems.

System	**c-cyt** $[\mu mol/g_{protein}]$	**SD** (σ)
L100F20	4.628	0.525
L70F50	4.040	0.514
L50F50	3.486	1.074
L50F70	2.993	0.839
L20F100	2.869	0.309

D.4 U(IV) and total uranium recovery concentrations over time during U(VI)-edta bioreduction for systems with different electron donor-acceptor ratios

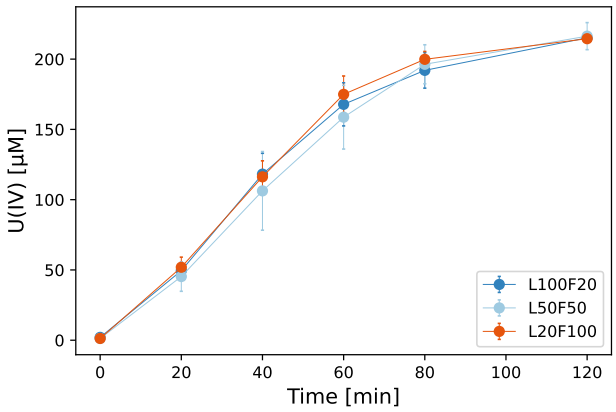

Figure D.3: U(IV) concentrations over time during U(VI)-edta reduction by *S. oneidensis* MR-1 wild-type grown in L100F20; L50F50 and L20F100 medium (numbers correspond to mM of lactate:fumarate respectively). Results correspond to the mean of replicate A and B, where error bars represent 2σ.

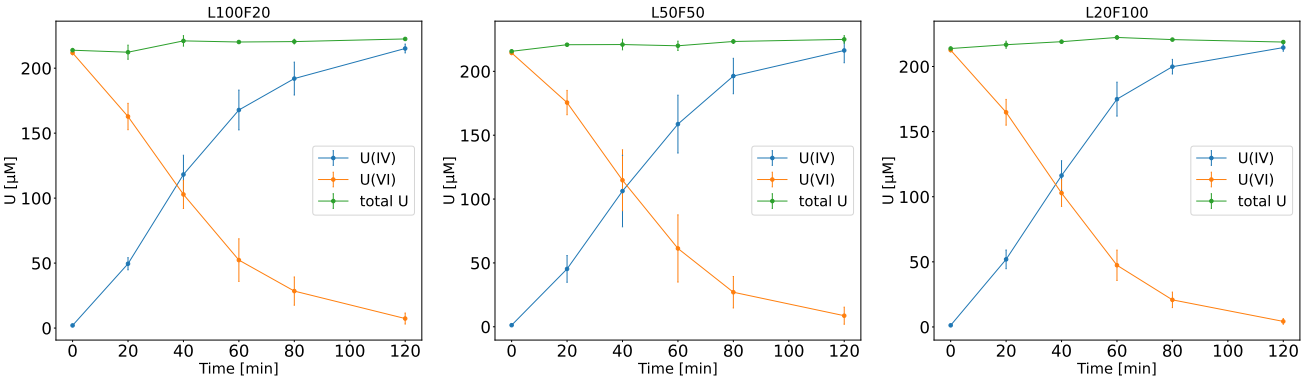

Figure D.4: Uranium recovery over time during U(VI)-edta reduction by *S. oneidensis* MR-1 wild-type grown in L100F20; L50F50 and L20F100 medium (numbers correspond to mM of lactate:fumarate respectively). Results correspond to the mean of replicate A and B, where error bars represent 2σ.

Appendix E

CymA and Fdh recombinant MR-1 experiment

E.1 U(IV) and total uranium recovery concentrations over time during U(VI)-edta bioreduction for cymA, cymAfdh and wild-type MR-1 recombinant

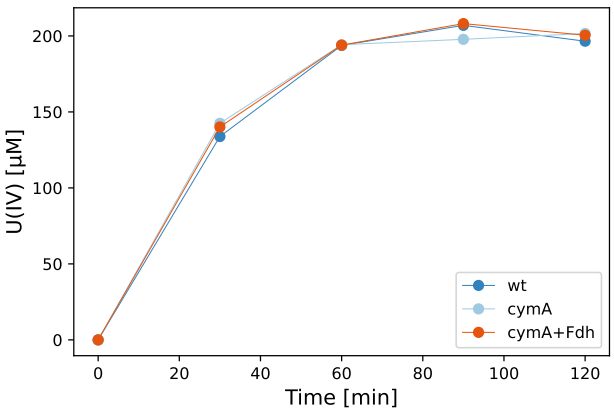

Figure E.1: U(IV) concentrations over time during U(VI)-edta reduction by *S. oneidensis* wild-type, CymA and CymA+Fdh MR-1 recombinant. Results correspond to replicate A only.

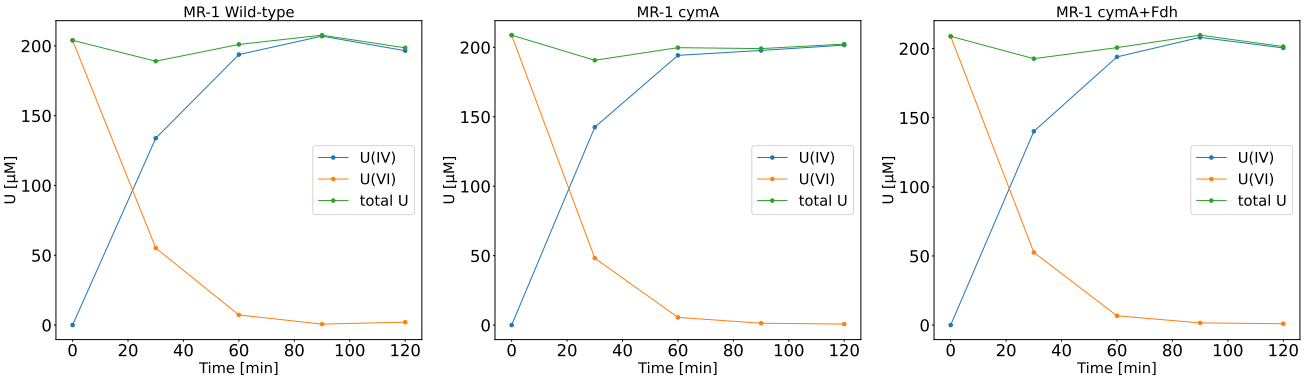

Figure E.2: Uranium recovery over time during U(VI)-edta reduction by *S. oneidensis* wild-type, CymA and CymA+Fdh MR-1 recombinant. Results correspond to replicate A only.

Appendix F

P_{BAD}-MtrCAB promoter experiment

F.1 U(IV) and total uranium recovery concentrations over time during U(VI)-edta bioreduction for MtrCAB strain in different L-arabinose concentrations

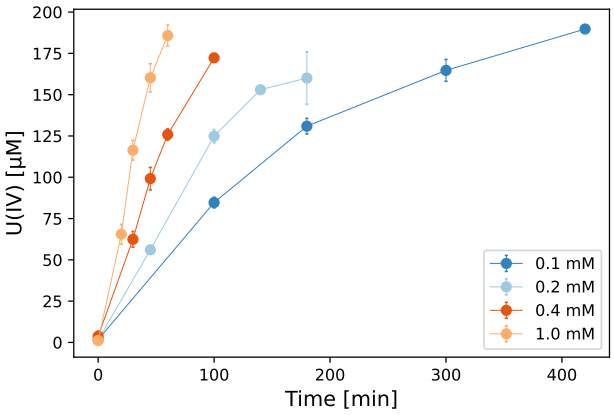

Figure F.1: U(IV) concentrations over time during U(VI)-edta reduction by P_{BAD}-mtr MR-1 strain grown in 0.1;0.2;0.4 and 1.0 mM of L-arabinose. Results correspond to the mean of replicate A and B, where error bars represent 2σ.

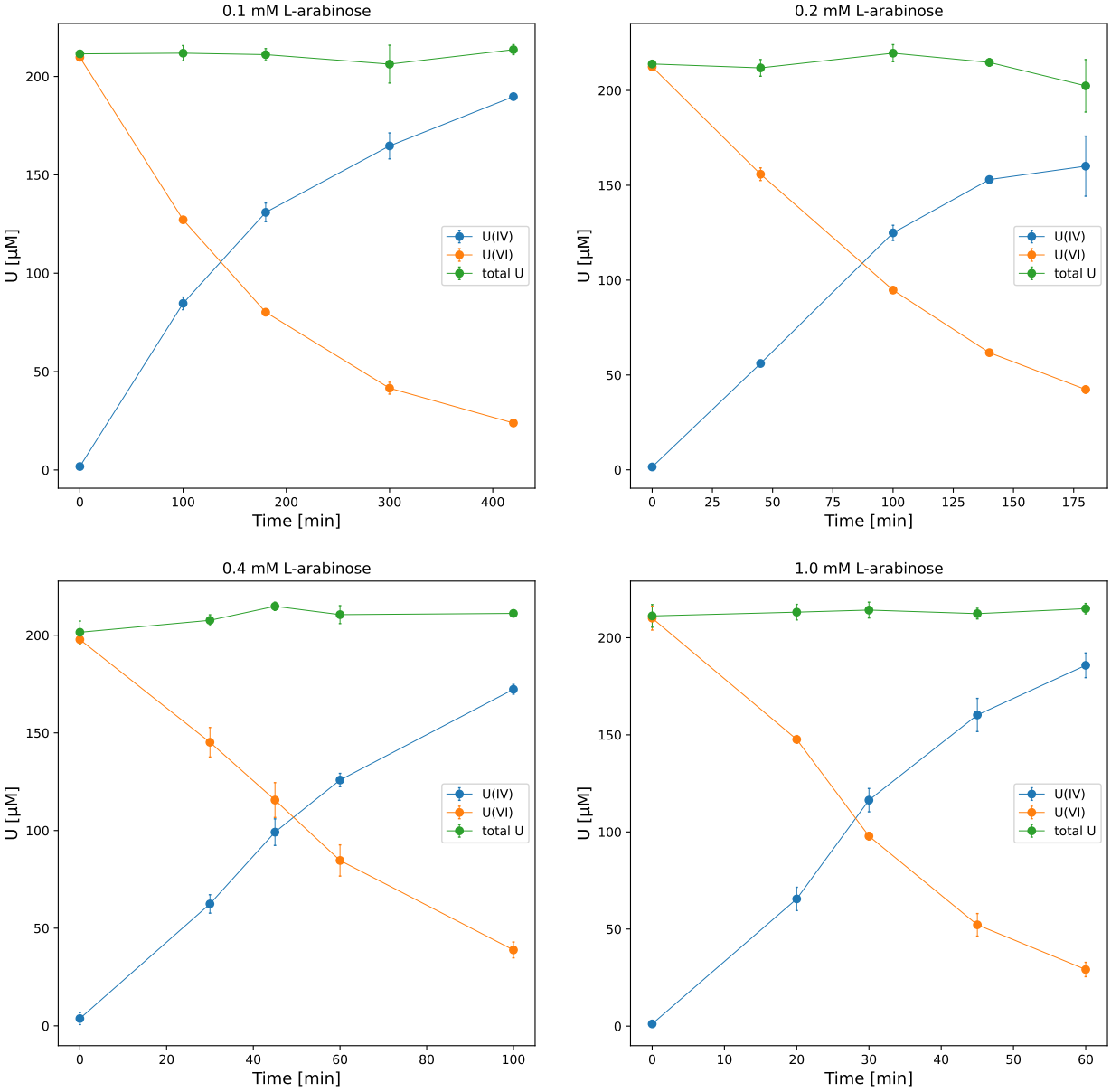

Figure F.2: Uranium recovery over time during U(VI)-edta reduction by P_{BAD}-mtr MR-1 strain grown in 0.1;0.2;0.4 and 1.0 mM of L-arabinose. Results correspond to the mean of replicate A and B, where error bars represent 2σ.

F.2 RT-qPCR results obtained for P_{BAD}-MtrCAB strains in different L-arabinose concentrations

Table F.1: Expression level for P_{BAD}-MtrCAB strains in different L-arabinose concentrations (replicate A) obtained from RT-qPCR analysis. Ratios are relative to control sample.

	[L-ara] mM	**expression ratio**	**negative SE**	**positive SE**
control	0.1	1	-	-
treatment	0.2	2.516	2.45	2.593
treatment	0.4	6.657	6.379	6.937
treatment	1.0	11.414	10.917	11.884

Appendix G

Impact of reaction rates on uranium fractionation

G.1 Isotope fractionation for model including all data points

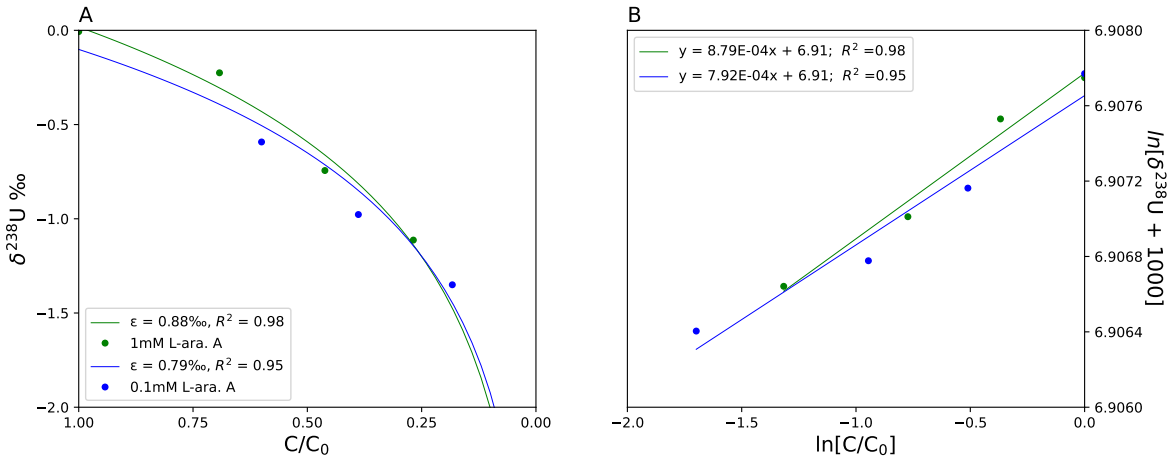

Figure G.1: First model obtained for isotope fractionation results using all data points, obtained for P_{BAD}-mtrCAB MR-1 strain grown in 0.1 and 1.0 mM L-arabinose (replicate A only). Panel (A) illustrates $\delta^{238}U$ values against unreacted fraction of U(VI), where ε values are reported. Panel (B) shows the Rayleigh distillation model fit for both systems